THE FLORIDA STATE UNIVERSITY

COLLEGE OF ARTS AND SCIENCES

INFORMATION CONTENT IN THE ERS-1 THREE-DAY REPEAT

ORBIT SCATTEROMETER WINDS OVER THE NORTH PACIFIC
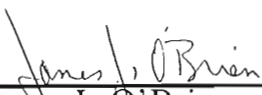
FROM JANUARY THROUGH MARCH 1992

By

PAUL T. BEAUDOIN

A Thesis submitted to the
Department of Meteorology
in partial fulfillment of the requirements
for the degree of Master of Science

Degree Awarded:
Summer Semester, 1994

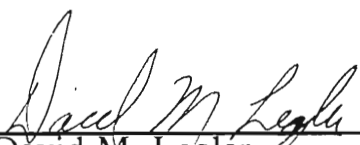The members of the Committee approve the Thesis of Paul T. Beaudoin, defended on May 23, 1994.

James J. O'Brien
Professor Directing Thesis

Eric A. Smith
Committee Member

Tiruvalam N. Krishnamurti
Committee Member

David M. Legler
Committee Member

To my wonderful wife, Helen, for all her love and support and to my precious daughter, Mary, for the joy she adds to both our lives.

Acknowledgement

I wish to express my sincere gratitude to Dr. James J. O'Brien, my major professor and thesis advisor. I have greatly appreciated his advice, support, and instruction during my course of study at Florida State University. I also wish to thank Dr. David M. Legler, thesis advisor and committee member, for his patience and instruction in the "art" of scientific writing.

I want to thank my wife and daughter for their love, support, and courage during this transitional period in our lives. Their inspiration and prayers have been the wind beneath my wings.

I want to thank my colleagues at the Mesoscale Air-Sea Interaction Group for their friendship and constructive comments and suggestions. Their team spirit adds an extra dimension to the learning process with the experience of successive graduates passed on to those just entering their graduate career.

Table of Contents

List of Tables

List of Figures

Abstract

This study examines ERS-1 three day repeat orbit scatterometer wind data from January through March 1992. The study region encompasses the north Pacific from 30°N to 50°N latitude and 160°E to 130°W longitude. The data are separated by orbit trajectory and binned to a 26 km by 26 km grid. These data are examined by direct comparative analysis to surface ECMWF model analyses on daily, monthly and three month time scales. The scatterometer wind fields compare favorably but distinct, non-isolated differences exist. These differences, exhibited in the scatterometer winds, include slightly stronger wind speeds, more distinct curvature, and detail on structures smaller then the ECMWF resolution. The scatterometer wind retrieval algorithm (CMODFD / NSCAT MLE) demonstrates some difficulty in selecting the true wind vector. Most of the difficulty appears to be related to upwind-downwind symmetry problems and are generally identifiable by inspection. Complex empirical orthogonal function (EOF) analysis on the ascending and descending scatterometer wind fields reveal frequency and amplitude information about the sampled variance. The first four EOFs, those for which the results suggest physically motivated phenomena, account for 50-60% of the total variance sampled in the data. The EOF results partition the sampled variance in the ascending and descending data and suggest the more significant EOFs depict spatial/temporal "bands" of 18-21, 8-10, and 6-8 days, sampled variance in the ascending and descending data and suggest the more significant EOFs depict spatial/temporal "bands" of 18-21, 8-10, and 6-8 days, reflecting the planetary wave cycle, large scale general circulation systems, and

xi

smaller scale storm structures; respectively. The partitioning of the variance

demonstrates only limited filtering capability in removing erroneous wind vectors.

1.   Introduction

Wind observations near the Earth's surface play a vital role in atmospheric forecasts. The wind transfers momentum and energy to the upper layers of the ocean and provides a substantial source of energy for a variety of oceanic processes. Therefore, the structure of the near-surface wind field over the ocean is of considerable interest.

The climatological mean wind field is fairly well established for the northern latitudes and tropical ocean. Climatologies such as (Hellerman and Rosenstein, 1983, Oberhuber, 1988, Wright, 1988, and Trenberth *et al.*, 1990) incorporate the National Climatic Center data set, TDF-11, containing millions of surface observations covering the world ocean from 1870-1976. Analyses of monthly (or more frequent) fields such as Halpern *et al.* (1993a) display the analysis of several·data sources including the Special Sensor Microwave Instrument (SSMI), buoy-drift, and European Center for Medium-Range Weather Forecasts (ECMWF) model output for the years 1988-1991. Others are specialized regional wind analyses, *e.g.*, Stricherz *et al.* (1993) which use all *in situ* data (ship reports, buoys, and other marine observing stations) in a variational direct minimization objective analysis for the Indian Ocean.

These averaged wind fields lack the detail necessary to resolve the shorter atmospheric scales associated with day to day wind patterns. These scales contain

atmospheric scales associated with day to day wind patterns. These scales contain significant energy and can be an important driving force in the dynamics of the

1

atmosphere and the ocean. Atmospheric global general circulation model, GCM,

output, as in the case of the ECMWF model, often assimilate data with analysis

algorithms imposing relatively heavy filters, thereby, loosing much of the detail found

in the original data. Evidence indicates, the incorporation of smaller scale, "high

resolution", wind fields can improve both oceanic and atmospheric model performance

(Satellite Surface Stress Working Group, 1992 and Anderson *et al.*, 1992) but

difficulty arises in establishing reliable winds fields, depicting a broad range of scales,

over shorter periods, *i.e.*, 1-30 days.

Ships, buoys, and other marine observing stations represent an irregular,

spatially and temporally limited, observation network. This network possesses only

limited capabilities for measuring small scale atmospheric features and lacks sufficient

density to produce high resolution wind fields with the bulk of the observations

confined to the major shipping lanes. Additionally, some *in situ* observations are

dominated by to mesoscale variability (atmospheric phenomena ranging from one to

tens of kilometers; *i.e.*, gust fronts, down bursts, etc., and possessing time scales of 1

hour to several minutes) These features are not resolvable by present GCM's. Satellite

borne scatterometer instrumentation provides a sensible solution to the limited

observational network providing near real-time area wind vectors over the world ocean

- irregularly sampled in time. These area wind vectors do not completely remove or

filter out the mesoscale, particularly over the ocean, where the low frequency end of

the mesoscale extends into the synoptic scale (Pierson, 1983). Numerous works

highlight the importance, validity, and application of remotely sensed winds; Brown

the mesoscale extends into the synoptic scale (Pierson, 1983). ....

highlight the importance, validity, and application of remotely sensed winds; Brown

2

(1983), Katsaros and Brown (1991), Estoque and Fernandez-Partagas (1983), Hoffman (1992), Freilich and Chelton (1986), Legler and O'Brien (1985), Legler and O'Brien (1993), Barnier *et al.* (1993) and Miles (1993) in addition to those previous mentioned.

The sampling characteristics (limited temporal coverage of the same location and temporal shifts between adjoining ground tracks) of satellite scatterometer winds complicate studies of the wind fields. The work of Freilich *et al.* (1986) analyzing the wave number spectra of Pacific winds derived from Seasat scatterometer data avoided the sampling problem by limiting the analysis to one dimension (along the satellite ground track). This study analyzes the two dimensional variability of the scatterometer wind field over the North Pacific and represents the first such work done for any portion of the Pacific utilizing ERS-1 scatterometer data.

In July 1991, the European Space Agency (ESA) launched the ESA Remote-Sensing Satellite, ERS-1, providing the first space-borne scatterometer data since Seasat in 1978. ERS-1 provides measurements of radar backscatter, σ^o, with empirical models supplying the relationship between σ^o and 10m winds. From January through March 1992, ERS-1 employed a three day repeat orbit representing the first time such an orbit has been used to produce active microwave instrument (AMI) winds. The frequency, multiple antenna design, and polarization technique used in measuring the radar backscatter provide a highly capable configuration less susceptible to signal degradation from precipitation as the Seasat and USAF DMSP satellites. The three day repeat orbit produces poor spatial coverage but represents an improvement to *in situ* measurements. The three day repeat orbit and the improved spatial coverage over *in* repeat orbit produces poor spatial coverage but represents an improve

measurements. The three day repeat orbit and the improved spatial coverage over *in*

3

situ data afford a unique opportunity to examine the information content of the ERS-1 scatterometer winds for synoptic scale features.

The focus of this study is to explore the information content of ERS-1 three day repeat orbit scatterometer wind vector data utilizing direct comparative examination and empirical orthogonal function (EOF) analysis. The study location provides a rich environment of synoptic scale features, *Fig 1-1*, as well as a limited number of *in situ* observations. This study capitalizes on the natural partitioning of the variance seen in the atmosphere (Boer and Shepherd, 1983) and highlighted in the analysis technique.
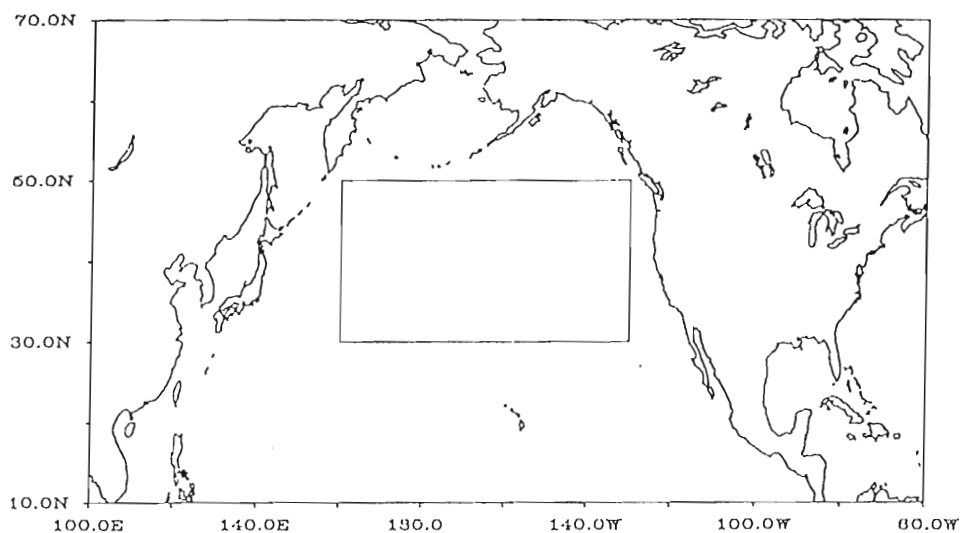
Fig. 1-1: Geographical region in the Pacific used for the present study.

The first part of results examine the information content in the scatterometer winds through two direct comparative analyses using ECMWF model analysis wind fields. The first comparison encompasses a direct correlation between the scatterometer winds through two direct comparative analyses using ECMWF model analysis wind fields. The first comparison encompasses a direct correlation between the scatterometer

4

winds and ECMWF model analyses with the model analyses linearly interpolated in time to match the scatterometer sampling times. The second comparison involves the correlation of monthly and three month vector averaged mean wind fields from both data sets.

The second portion of the results examine the partitioning of the variance exhibited in the EOF analysis. The EOF analysis methodology allows for "filtering" of the data based on the individual EOF contributions to the total variance exhibited in the system. The study examines the individual EOFs and suggests physically motivated phenomena for the first few significant EOFs and explores the capability of the EOF analysis in filtering out erroneous wind vectors. Additionally, the study explores the combination of ascending and descending wind vectors (separated by 12 to 60 hours) using a vector average of the EOF reconstructed wind field. A more complete discussion of the study results follows a brief description of the North Pacific climatology, data and analysis methods.

2.   Winter Climatology of North Pacific Winds

The study period, January-March, represents a period of highly active transient cyclonic activity. The winter, mean sea-level pressure distribution over the North Pacific highlights a general zone of subpolar low pressure, commonly referred to as the Aleutian Low, centered north of the Aleutian island chain and south of the Bering Strait. The presence of the low pressure zone on mean pressure maps depicts the passage of deep depressions across the region downstream of the upper air long-wave trough. Major storm tracks pass through the western boundary of the study region, *Fig 1-1*, and migrate along the northern border of the study region. Several secondary storm tracks originate within the interior of the study region and exit through the northeastern section of the study region into the Gulf of Alaska before continuing into North America (Barry and Chorley, 1987).

The structure of the mean wind field as presented by Wright (1988) resembles a geostrophic approximation to the mean sea-level pressure patterns with strong winds (6-8ms⁻¹) in the western area generally decreasing in strength (< 2ms⁻¹) towards the southeastern portions of the study region. These results are not surprising, the Kuriosho influences the western portion of the study region through the introduction of warm water aiding in the development and/or enhancement of storm systems. The stronger mean winds illustrate the relatively frequent and stronger storm systems warm water aiding in the development and/or enhancement of storm systems. The stronger mean winds illustrate the relatively frequent and stronger storm systems evident in the region. Weaker winds characterize the southeastern portion of the study

6

region and represent the influence of a weak subtropical high pressure cell. This cell of the subtropical high pressure belt strengthens through the study period and provides the only exception to the generally zonal character of the mean winds over the North Pacific during the study period.

3.   Data

ERS-1 mounts a suite of instrumentation for the expressed mission objective of remotely sensing the Earth. The wind scatterometer, employing a 5.3-GHz (C-Band) signal, accounts for one of two radars comprising the Active Microwave Instrument (AMI) and is referenced as the wind mode of the AMI. The other radar, a synthetic aperture radar (SAR), provides either high resolution radar imagery (image mode) or information on sea surface wavelengths and direction (wave mode). Power requirements prevent the operation of the AMI in all three modes (wind, wave, and image), concurrently. Further, radar imagery excludes operation in the wind mode although wind/wave operations may operate in an interleaved fashion. Therefore, mission objectives may prevent scatterometer measurements through the course of an orbit.

The ERS-1 satellite employs a sun synchronous polar orbit with an inclination of 98.5°. Pertinent orbital parameters include a descending equatorial node at 1030 local time, a nominal altitude of 785km, and repeat orbits of 3, 30, and 176 days through slight altitude adjustments. The European Space Agency (ESA) maintains the orbital parameters to produce a ground track repeatability to within ±1km at any point in the orbit.

The wind scatterometer employs three sideways viewing antennae, one pointing in the orbit.

The wind scatterometer employs three sideways viewing antennae, one pointing normal to the satellite flight path and one each pointing 45 degrees forward and

8

backward. While in wind mode, the radar beams continuously illuminate a swath 500 km wide and 200km to the right of the nadir path. Each antennae measures the strength of the resonant Bragg scattering produced from approximately 5-cm wave length capillary surface waves for an overlapping 50km diameter foot print and a 25km pixel spacing. This produces three independent backscatter measurements, σ^o, at cell center nodes on a 25km grid separated by only a very short time delay. Calculation of the surface wind vector in terms of speed and direction uses these "triplets" within an empirical model relating σ^o, wind direction, and incidence angle of the observation. Brown (1983) provides a detailed description of the process as applied to the SEASAT-A scatterometer.

The amplitude and density of the capillary waves depend upon the wind speed and directly affect the strength of the return signal. The wind direction strongly influences the shape of the waves but the details defining these relationships represent some of the most challenging problems in geophysical fluid dynamics; stability, wave generation, and wave propagation and interaction theories. The mechanics of wind generated waves remains one of the fundamental unsolved problems of fluid dynamics. The interaction of the short gravity waves and capillary waves with longer waves remains a significant and complex obstacle as is the relation between the 10m wind and the momentum flux into the ocean surface. Rain, white caps, and breaking waves remains a significant and complex obstacle as

and the momentum flux into the ocean surface. Rain, white caps, and breaking waves further complicate the problem [Brown, 1983]. Additionally the problem associated

9

with atmospheric attenuation, principally due to rain, deteriorates the return signal, thus significant uncertainties exist in scatterometer data.

Despite the formidable obstacles complicating the use of scatterometer σ^o measurements, several empirical methods provide tractable solutions. This study utilizes the January - March 1992 V-A data product distributed by JPL and generated from re-processing σ^o with the Freilich and Dunbar (1992) model function (herein referred to as CMODFD) coupled with the National Aeronautics and Space Administration (NASA) Scatterometer (NSCAT) maximum likelihood estimation (MLE) retrieval algorithm. CMODFD is an empirical C-Band scatterometer model function relating σ^o to surface wind velocity (speed and direction) over a full range of incidence angles, speeds, and azimuths. The functional relationship, or model function, is expressed in the form of a cosine expansion about the wind azimuth,

$$\sigma^o \ (|U|, \ \theta) \ = \ A_0 \ + \ A_1 \ COS(\chi) \ + \ A_2 \ COS(2\chi) \tag{3.1}$$

$|U|$ = wind speed, θ = incidence angle, and $\cdot$ χ = wind azimuth.

The coefficients are determined through the correlation of the return signal to collocated comparison wind data for the first six months of 1992. Comparison wind data were primarily high resolution global surface wind analyses produced by the U.S. National Meteorological Center (NMC). In the process of computing wind speed and direction, the model function typically produces a set of wind vector solutions or ambiguities, generally possessing similar magnitudes but deviating extensively in direction. These ambiguous solutions result from symmetries in the model function but

ambiguities, generally possessing similar

direction. These ambiguous solutions result from symmetries in the model function but only one wind vector solution corresponds to the true solution, the others are generally

aliases. The NSCAT MLE algorithm is used as an ambiguity selection scheme. The MLE algorithm is in the form of a joint probability density function and assumed to be directly proportional to the likelihood that a particular ($|U|$, θ) solution corresponds to the true wind speed and direction (Schultz, 1990).

CMODFD represents an improvement to the Stoffelen and Anderson (1992) model function (herein referred to as CMOD2) employed by ESA (prior to 1993) and used to provide original ERS-1 ESA wind vectors for the analysis period. Halpern *et al.,* (1993b) evaluated the two C-Band model functions (CMOD2 and CMODFD), concluding CMODFD more accurately represented the 10-m height wind vector field. The average rms difference and average correlation coefficients between the monthly mean and daily averaged CMODFD and moored-buoy matchups of the cartesian wind components were 1.25 m/s and 0.84 (monthly) and 3.0 m/s and 0.74 (daily averaged). Halpern *et al* (1993b) listed three factors contributing to the conclusion that CMODFD more accurately represented the near-surface winds than CMOD2 (*i*) CMOD2 does not produce winds below 4m/s, (*ii*) the CMODFD wind vectors more accurately portrayed the climatological-mean wind systems over the Pacific Ocean, and (*iii*) CMODFD more strongly corresponded to moored-buoy data.

As mentioned previously, this study utilizes the CMODFD processed winds with the NSCAT selected ambiguity for the period, January through March 1992. This study considers only scatterometer winds computed during optimal satellite operational status, *e.g.*, winds computed from only two σ° values instead of the three nominally available, during antennae arcing, or during signal threshold limitations are *not* used in

11

this study. The January - March study period was the first scheduled three day repeat orbit portion of the ERS-1 program. The spatial coverage produced in any one day of the three day repeat orbit exhibits large horizontal gaps in the study region. The horizontal gap for successive passes varies from approximately 25° longitude at the equator to overlapping sample areas beyond 79° latitude. In contrast, the spatial coverage produced over the three day repeat orbit provides an extremely dense network, *Figs 3-1 and 3-2*, particularly in comparison to ship and buoy data over the study region for the entire three month period (28,000+ possible satellite observations in a *three day* period compared to 21,000+ *in situ* observations for the entire *three month* period).

Though capable of 28,000+ observations (14,000+ each for both ascending and descending orbital trajectories) over a three day period throughout the study region, scatterometer wind data availability throughout the study period suggests mutually exclusive mission requirements, intermittent technical difficulties, and/or signal calibration. As mentioned previously, the wind scatterometer represents one of two radars comprising the AMI and while in image mode, scatterometer winds are unavailable. ESA routinely produces technical notes (*e.g.*, Amans and Marcorelles, 1993) documenting AMI unavailability since launch, but this accounts only for approximately 5% of the missing observations. The present study does not posses the additional documentation detailing mission profiles (Image <u>vs</u> Wind mode) and the operational status of the individual antennae to account for the remaining missing observations.

12
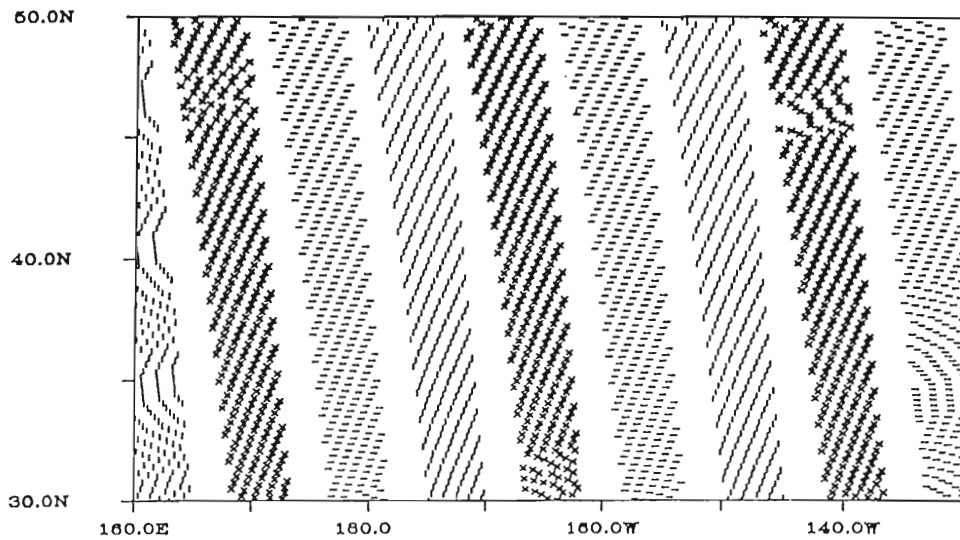
Fig 3-1: Sample coverage from ascending orbits of ERS-1 scatterometer wind data (using CMODFD), 22-24 March, with every 5th measurement plotted illustrating daily coverage; (-) first, (l) second, and (x) third day of the cycle.
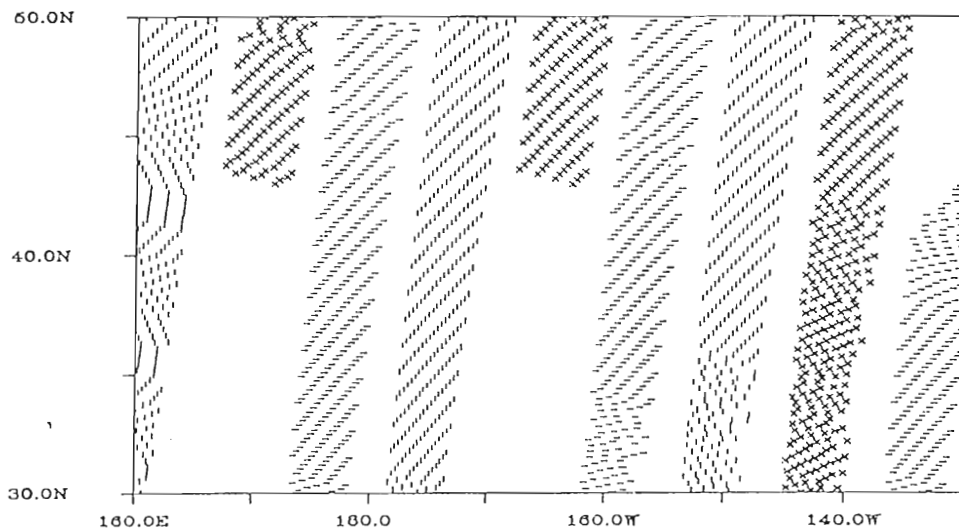
Fig 3-2: Sample coverage from descending orbits of ERS-1 scatterometer wind data (using CMODFD), 4-6 March, with every 5th measurement plotted illustrating daily coverage; (-) first, (l) second, and (x)

This study employs two additional wind vector data sets for comparative purposes, the European Center for Medium-Range Weather Forecasts (ECMWF) / Tropical Ocean Global Atmosphere (TOGA) Advanced Operational Data Set and *in situ* observations (primarily ship reports, assumed to be measured at 19 meters height). The ECMWF/TOGA data are operational model analyses (provided in support of the TOGA program) and include numerous global products. The 10 meter longitudinal (u) and meridional (v) wind components from the Surface and Diagnostic Fields Data set are available four times daily at 00Z, 06Z, 12Z, and 18Z on a 1.125 by 1.125 degree resolution. *In situ* observations used in this study come from the COADS (Slutz, 1985) and constitute all individual observations in the study region over the three month period. To match the ECMWF/TOGA wind fields, this study computes fields of the *in situ* observations on a 1.125 by 1.125 degree grid.

4. Analysis Methodology

The analysis procedure employed in this study consists of four components; preparation of the data arrays, Empirical Orthogonal Function (EOF) analysis, comparative analyses of the scatterometer winds with independent wind vector data sets (*Section* 5.1), and physical interpretation of the first few significant EOFs (*Section* 5.3). This section discusses the preparation of the analysis arrays, highlighting the development and basis, and the EOF analysis.

4.1 *Preparation*

In preparation for analysis, the scatterometer observations are sorted by trajectory (ascending and descending orbits) and separated into three day repeat orbits or cycles with the longitudinal and meridional components of the wind vector combined into its complex representation. The treatment of separate ascending and descending fields avoids the problems associated with combining the information content of two or more collocated wind vectors spanning 24+ hours. This obstacle arises from the nonuniform sampling characteristics of the three day repeat orbit.

The satellite wind vectors are assigned to a horizontal array of uniformly distributed grid points. This assignment process maps satellite observations onto nonoverlapping, 26 by 26 km elemental areas with the origin of the gridded array resting at 30°N, 160°E. This grid produces a relatively minor number of elemental nonoverlapping, 26 by 26 km elemental areas with the origin of the gridded array resting at 30°N, 160°E. This grid produces a relatively minor number of elemental areas with multiple wind vector observations over a given three day repeat cycle. The

15

multiple observations occur within the same orbit (generally 4 to 8 seconds separation in sampling time) and are arithmetically averaged to produce a resultant wind vector for the elemental area. This array preserves the both integrity of the satellite ground track and information content of the wind vectors.

The choice of grid scale stems from a data density study designed to maximize the spatial and temporal coverage for both ascending and descending fields. The results of the density study validate ground track repeatability and illustrate maximum spatial and temporal coverage using the 26km grid spacing for both the North-South and East-West directions. The 26 km grid resolution closely approximates the satellite pixel spacing (utilizing 96+% of the available scatterometer observations to cover ~70% of the study region) and provides an optimal balance between resolution and repeat observations. Additionally, the findings highlight areas of the study region (by orbit trajectory) exhibiting poor temporal coverage and illustrate overlapping ascending and descending spatial coverage *Figs 4-1 and 4-2* . This additional result coupled with an awareness for the regional climatology accounts for differences in the ascending and descending EOF patterns. Basically, the descending fields do not sample the variability in the western region because of poor sampling in this area.

For reasons discussed in the previous section, data scarcity severely limits the temporal densities available for the study. Simply stated, a temporal density defines the set of spatial grid points exhibiting a minimal number of repeat observations. There is a maximum of only 30 observations in time for each grid point (*i.e.*, 30 x 3 day repeat orbit = 90 days), hence, a temporal density of 18 refers to the spatial array There is a maximum of only 30 observations in time for each grid point (*i.e.*, 30 x 3 day repeat orbit = 90 days), hence, a temporal density of 18 refers to the spatial array

of grid points containing observations in 18 *or more* three day repeat cycles, *Figs 4-1 and 4-2*. Results show the selection of a temporal density of 18 optimizes spatial coverage. Further decreases in the temporal density selection produce minimal increases in spatial coverage with the descending orbits exhibiting generally poor temporal coverage in the western half of the study region (less than 10 observations during the three month period).

The preparation portion of the analysis procedure concludes with the development of a complex, two dimensional analysis array (space and time) for each orbit trajectory. The study addresses missing data through the removal of the time average mean from all points and then substituting zeros for absent observations (Jones *et al.* 1993). This produces the two dimensional analysis arrays, D_A (ascent) and D_D (descent), of the ERS-1 scatterometer data for use in the EOF analysis.

4.2 *Empirical Orthogonal Function (EOF) Analysis*

EOF analysis, also known as Principle Component Analysis, provides a methodology (*e.g.*, Preisendorfer, 1988) for evaluating the linked spatial-temporal patterns of the winds. The goal of EOF analysis is to represent the data as a set of spatial fields modulated by orthogonal basis functions (here after referred to as EOFs). These EOFs partition the variance of the data. The first few patterns, accounting for the highest percentage contributions to the total system variance, can often be related to identifiable, physically-motivated phenomena. The discussion to follow is, at best, only a cursory description of the mathematics involved in EOF analysis of two

to identifiable, physically-motivated phenomena. The discussion to follow is, at best, only a cursory description of the mathematics involved in EOF analysis of two
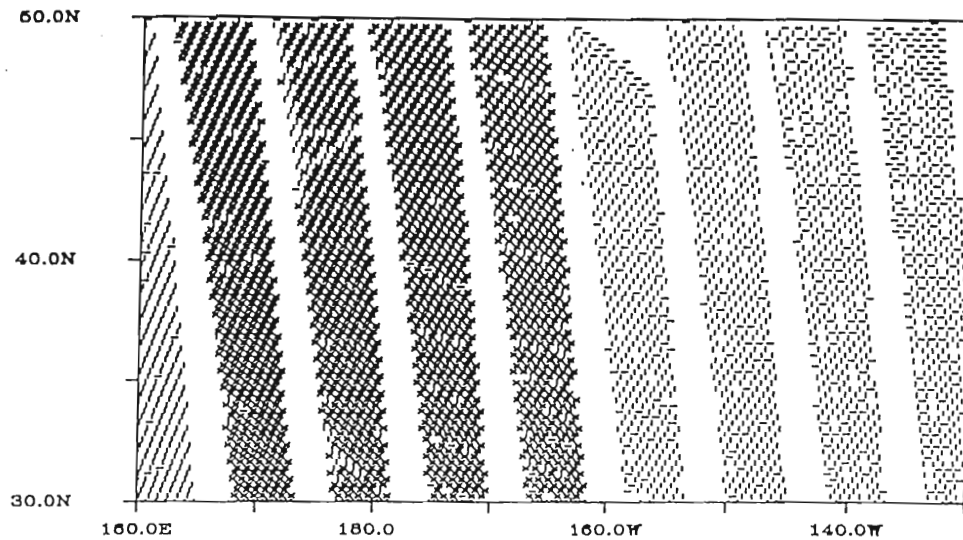
Fig 4-1: ERS-1 Scatterometer ascending orbit data density for Jan 1 - Mar 30, 1992. Temporal densities indicated as follows; (x) 21+, (l) 18-19, and (-) 15-17 with every 3rd elemental area plotted.
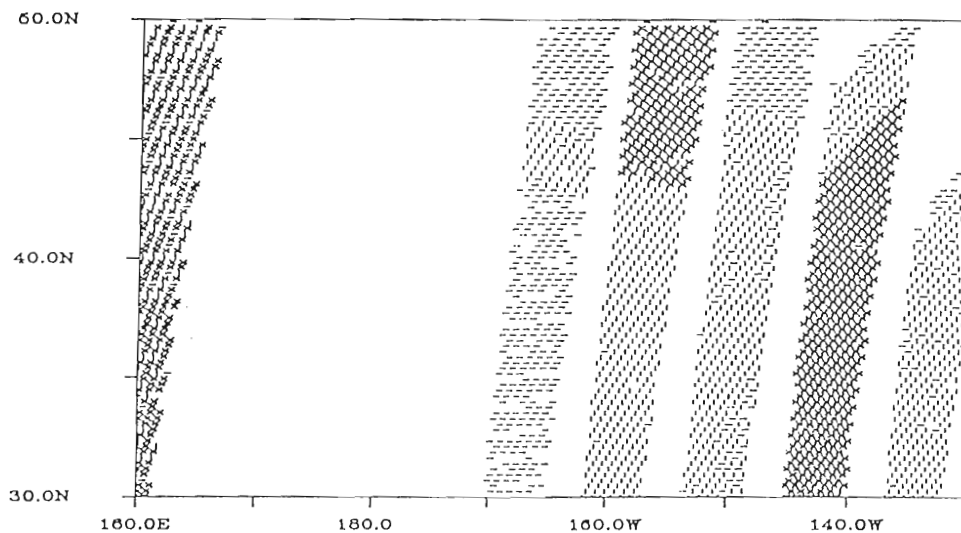
Fig 4-2: ERS-1 Scatterometer descending orbit data density for Jan 1 - Mar 30, 1992. Temporal densities indicated as follows; (x) 21+, (l) 18-19, and (-) 15-17 with every 3rd elemental area plotted. The blank area in the western half indicates there were less than 15 scatterometer values from the descending orbits during the analysis period. Temporal densities indicated as follows; (x) 21+, (l) 18-19, and (-) 15-17 with every 3rd elemental area plotted. The blank area in the western half indicates there were less than 15 scatterometer values from the descending orbits during the analysis period.

18

dimensional vector fields. For a more comprehensive discussion, the reader is referred to Preisendorfer (1988). Legler (1983) developed the method for wind vectors used here.

The EOF analysis procedure for the ERS-1 data begins with the computation of the ascending and descending Hermitian spatial covariance matrices, C_A and C_D respectively,

$$C_{A/D} = \frac{1}{N} (D_{A/D}^T \cdot D_{A/D}) \tag{4.1}$$

where N represents the number of spatial points and $(\ )^T$ represents the complex transpose. The mathematics of the EOF procedure separate the input data array into temporal, T, time series which modulate the spatial fields, S ;

$$D_{A/D} = S_{A/D} \cdot T_{A/D}^T \tag{4.2}$$

The temporal component, T, are complex time series (amplitude and phase). The basis functions arise from the eigensystem solution as the eigenvectors;

$$C_{A/D} \cdot T_{A/D} = \lambda_{A/D} \ T_{A/D} \tag{4.3a}$$

or

$$S_{A/D} \cdot D_{A/D} \cdot D^{T_{A/D}} = \lambda_{A/D} \ S_{A/D} \tag{4.3b}$$

Obviously any multiple of the eigenvector T will also be an eigenvector, but not distinct. Clearly equation (3a) can hold only if

$$Det \ | \ C_{A/D} - \lambda_{A/D} \ I \ | \ = \ 0 \tag{4.4}$$

distinct. Clearly equation (3a) can hold only if

$$Det \ | \ C_{A/D} - \lambda_{A/D} \ I \ | \ = \ 0 \tag{4.4}$$

In the expansion of equation (4), a Nth degree polynomial in λ is created whose roots are the eigenvalues (Press *et al.*, 1992). The normalized eigenvalues are,

$$\Gamma_i = \frac{\lambda_i}{\Sigma_{j=1}^{J} \lambda_j} . \tag{4.5}$$

They represent the contribution (percent variance) of the associated time series, T_i, and spatial field, S_i, to the total variance of the system. A spatial component, S_j, is computed from the "projection" of the T_j on the original data;

$$D_{j\,A/D} \cdot T_{j\,A/D} = S_{j\,A/D} \tag{4.6}$$

Thus from our data, 30 eigenvectors (actually 30 complex time series) and 30 spatial fields are created.

As a check of the calculation, the study calculates a root-mean-square (rms) estimate for estimating the difference, E, between the data, $D_{A/D}$, and the EOF reconstruction of the data, D_{EOF}, using all thirty eigenvectors and associated spatial fields;

$$E = \sqrt{\frac{(D_{A/D} - D_{EOF})^2}{(P \cdot N)}} \tag{4.7}$$

where P is the number of spatial points. As expected, the error for both ascending and descending EOF analyses is order (10^{-5}). The study utilizes the LAPACK (Linear Algebra PACKAGE) and BLAS (Basic Linear Algebra Subprograms) FORTRAN libraries in the solution of the eigensystem, development of the spatial fields, and EOF reconstruction of the analysis field.

reconstruction of the analysis field.

5. Results

5.1 *Direct Comparative Analysis of ECMWF and ERS-1 Scatterometer Winds:*

The study directly compares scatterometer winds to the ECMWF operational model analysis. A linear interpolation in time of the ECMWF analysis fields is produced to facilitate a reasonable comparison between the data sets more closely matching ERS-1 scatterometer sampling times. (Throughout the remaining portion of this study, reference to ERS-1 model analyses at other than 00, 06, 12, and 18Z refers to model analyses linearly interpolated in time.) The complete comparative analysis period includes 1-10 January and 1 February - 30 March. Due to the generally poor data availability of ERS-1 scatterometer winds (discussed in Section 3), the study omits the period 11-30 January for both the ascending and descending orbits trajectories. The dissimilar array formats (ECMWF is on a 1.125 by 1.125 degree grid array and scatterometer on 26 by 26 km grid array), the uneven sampling characteristics of satellite observations, and data density differences prevent simple quantitative comparisons.

Qualitatively, the comparisons illustrate remarkably good agreement in both speed and direction. This agreement includes frontal/trough placement, cyclonic patterns, and coll positions through a wide range of wind speeds, *e.g. Figs. 5-1 and 5-2*, preserving most of the kinematic structure. The comparisons also illustrate several

21
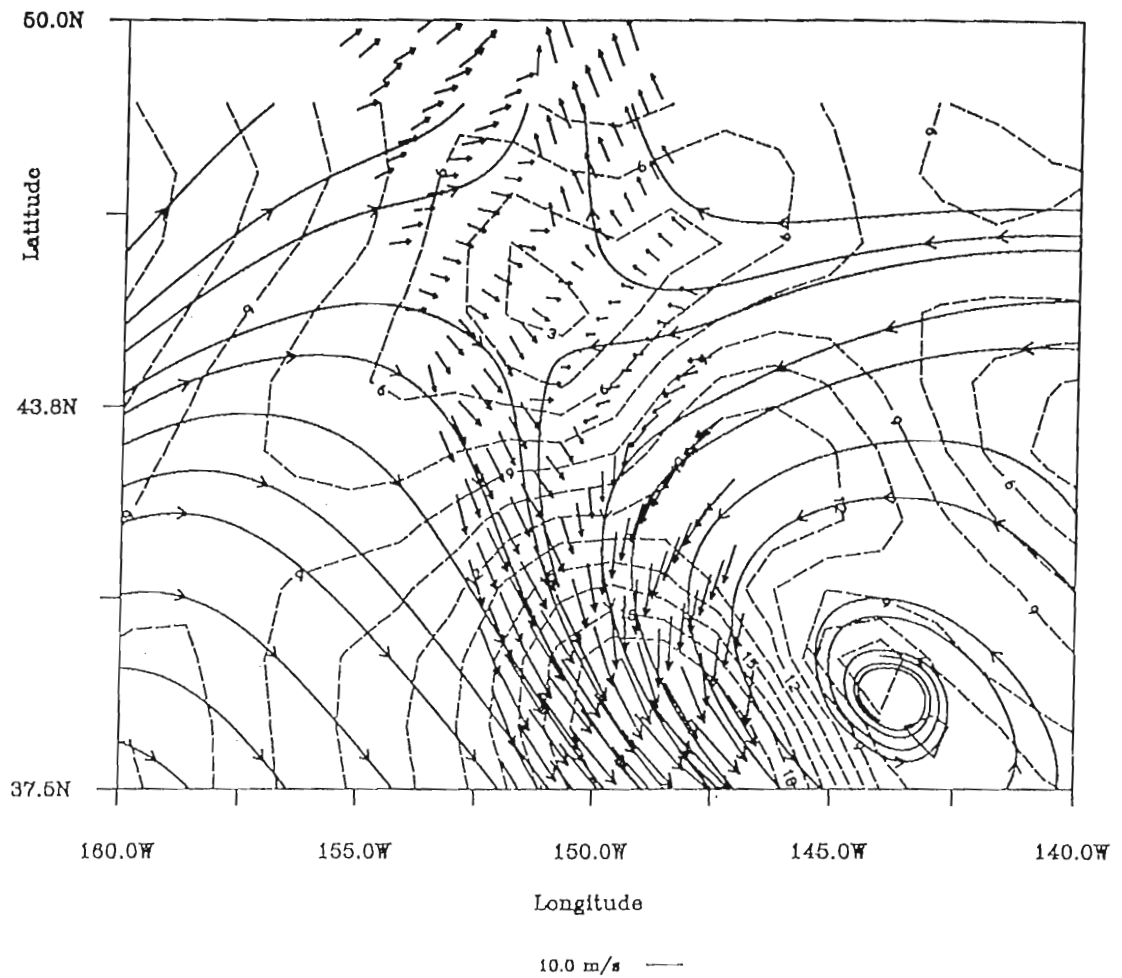
Fig. 5-1: Comparison field, 08Z 23 March 1992. ERS-1 scatterometer derived winds overlaying a stream line analysis of ECMWF/TOGA 10m wind analysis fields interpolated to the same time. ERS-1 overlay illustrates every 5th wind vector.
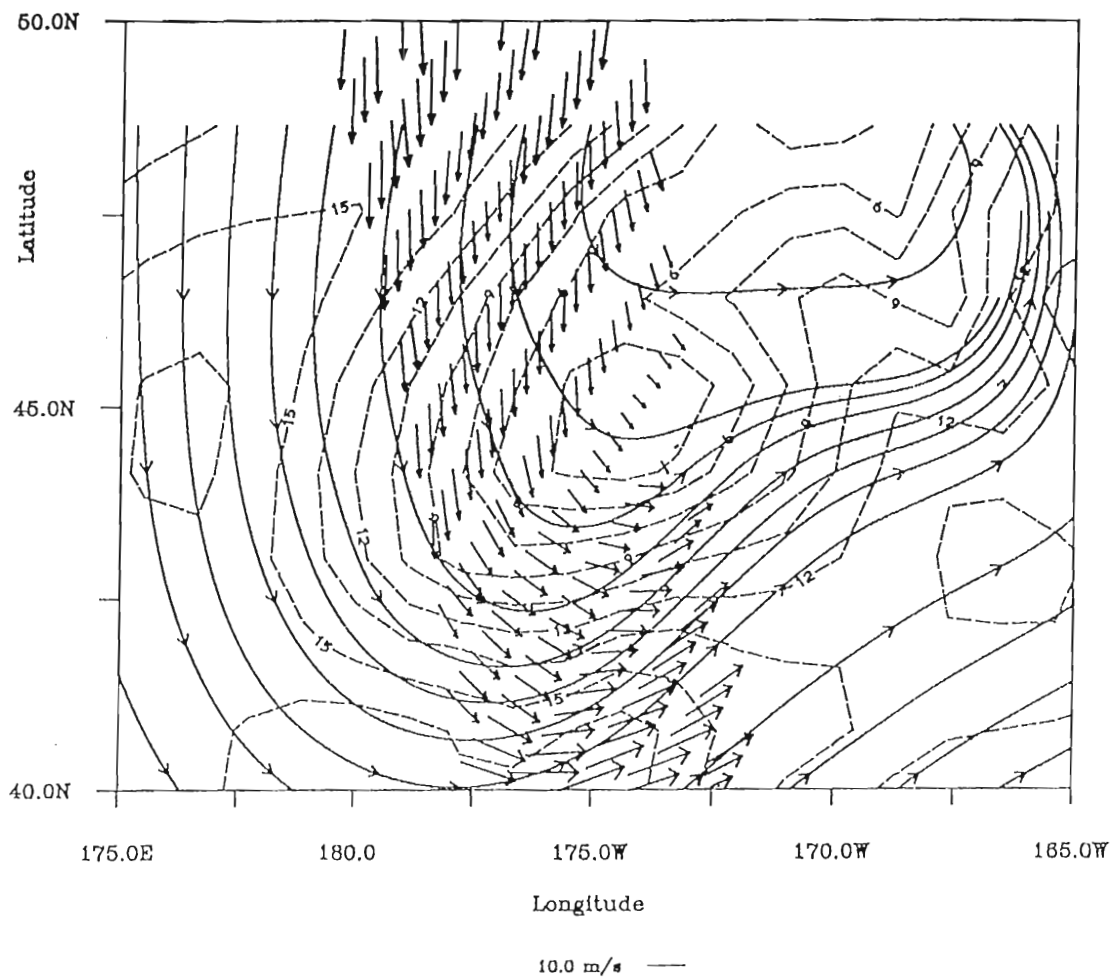
Fig. 5-2: Same as *Fig.* 5-1, for 10Z 29 March 1992.

characteristic differences evident in the ECMWF and ERS-1 fields. They are the definition or definability of small scale features, the center positioning of cyclonic flow, and the wind speed structure associated with coll and cyclonic patterns.

As expected, the higher resolution of ERS-1 scatterometer wind fields provide information on features beyond the resolution and/or adds detail to existing features of the ECMWF analysis fields. Previous studies involving assimilation of scatterometer data (*e.g.*, Anderson *et al.*, 1987) note the ECMWF assimilation process exacts a heavily toil on small scale features (where much of the new information exists) to ensure computational stability. The resultant ECMWF wind fields demonstrate a considerable measure of smoothness. Much of the differences in spatial scale resolvability exist at length scales smaller than 200 km and emphasize the physical ECMWF analysis limitations as dictated by the Sampling Theorem. *Fig. 5-3* exemplifies the type of small scale feature resolved in the scatterometer wind fields, highlighting a minor trough near 44° N on the order of 1° in size. Kinematically, the trough illustrates a low-level (near-surface) confluence zone. Though of little consequence to the synoptic pattern, small scale features such as these may highlight small regions where sufficient lifting exists in the moist ocean-atmosphere boundary environment to trigger mesoscale convective activity. *Fig. 5-4* depicts enhanced detail of the wind field provided by ERS-1 data. Comparison of the 10Z (approximate time) environment to trigger mesoscale convective activity. *Fig. 5-4* depicts enhanced detail of the wind field provided by ERS-1 data. Comparison of the 10Z (approximate time) field on 1 February suggests the ECMWF analysis either missed all together, mis-
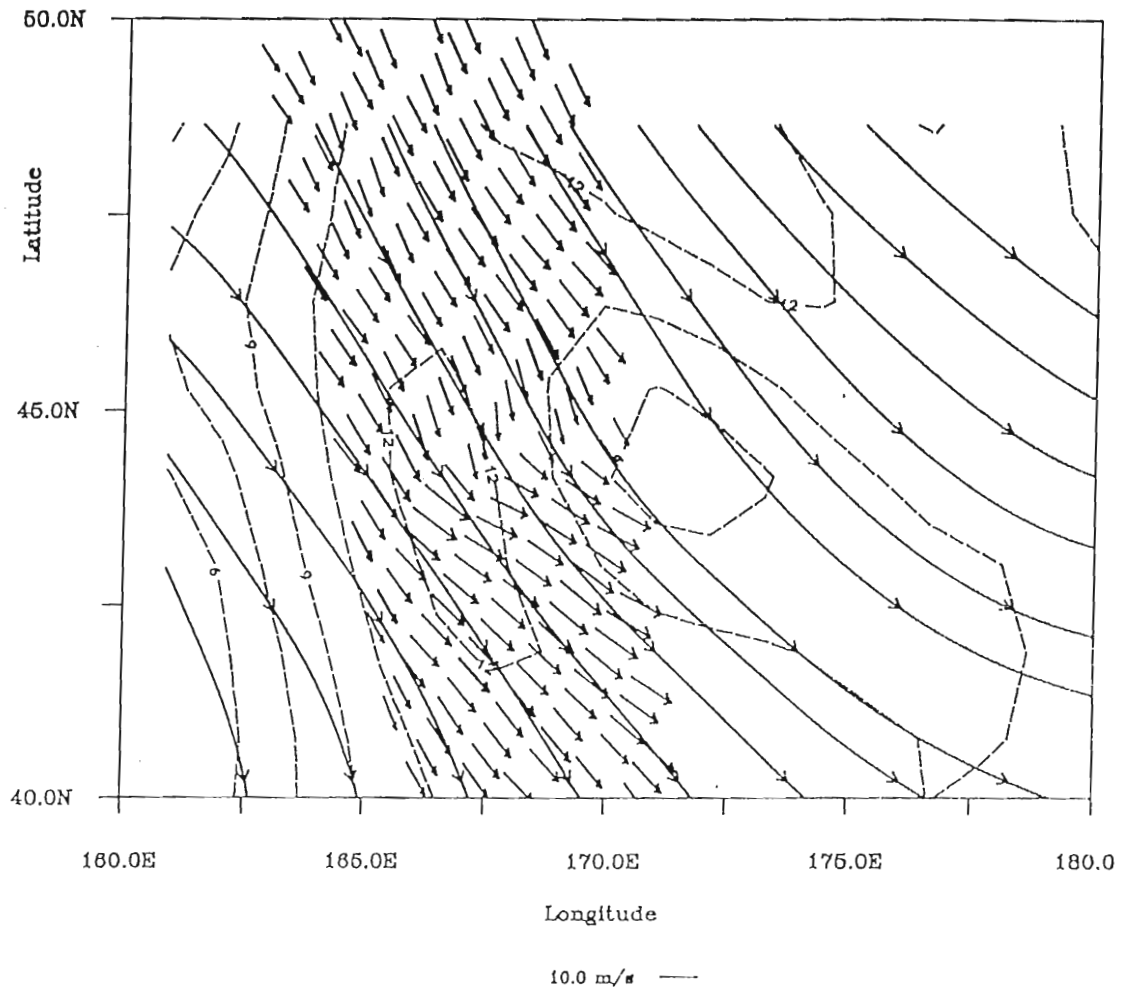
24

Fig. 5-3: Comparison field, 11Z 18 February 1992. ERS-1 scatterometer derived winds overlaying a stream line analysis of ECMWF/TOGA 10m wind analysis fields interpolated to the same time. ERS-1 overlay illustrates every 5th wind vector.
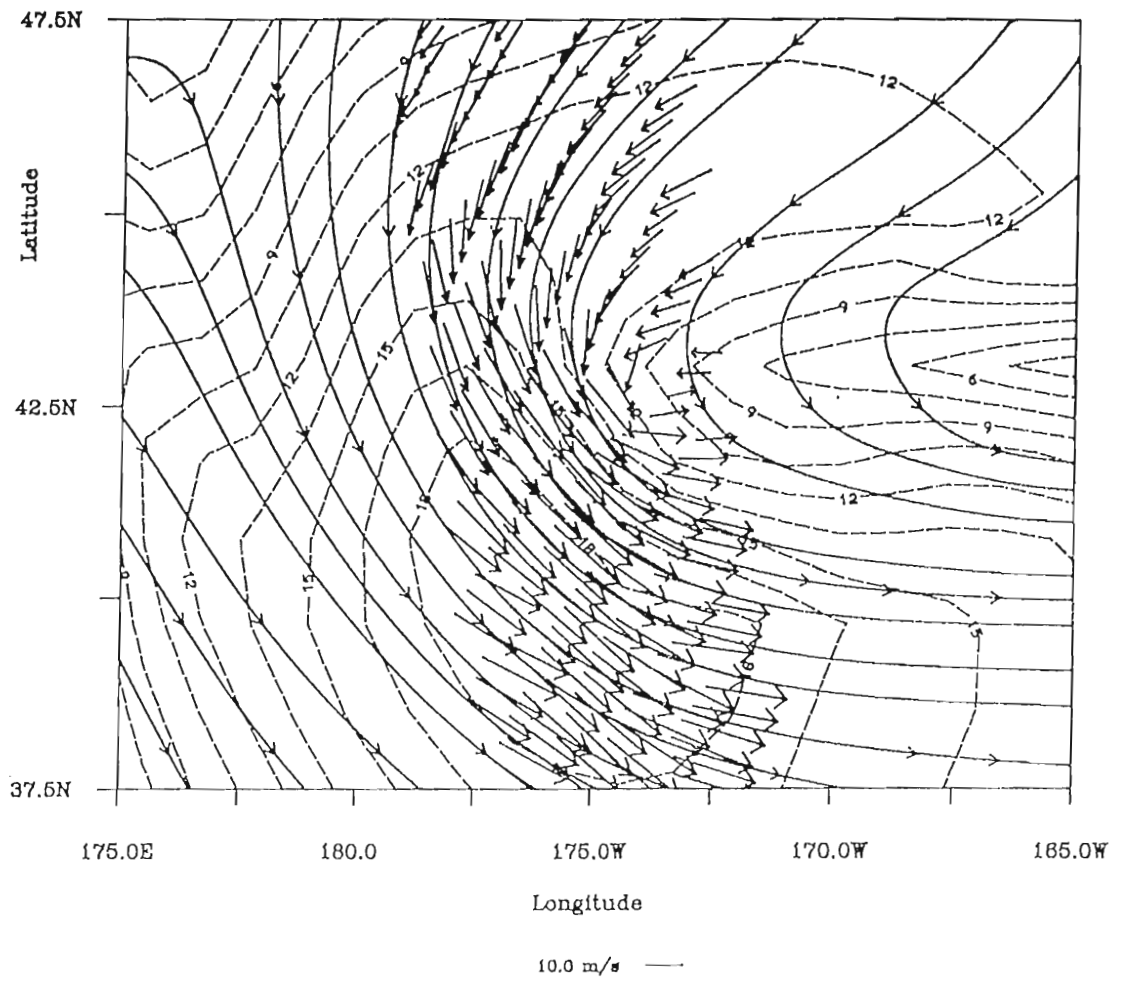
Fig. 5-4: Same as *Fig. 5-1*, for 10Z 1 February 1992.

interpreted, or incorporated the small cyclonic feature displayed in the scatterometer wind field into a much broader trough evident in the region. This much broader trough is positioned approximately 2° north of the small cyclonic feature. As in the previous example, this small scale feature is smaller than the ECMWF spatial resolution (this feature is approximately 1.5° by 1.5°).

The comparative results highlight position differences for cyclonic centers depicted by the two wind fields. These differences are typically found in the ascending data and are not isolated to a few cases. The scatterometer-located centers are south of the ECMWF-located centers (illustrated in *Fig. 5-5*). The displacement varies between cyclonic patterns and ranges from 1-3 degrees latitude. It is further noted, the study finds no situations in which the scatterometer derived center position is north of the position presented in the linearly interpolated ECMWF fields. The outer boundaries of the cyclonic flow field (2-3 degrees from the center of the cyclones) compare favorably. The study results note this difference in center positioning in 16 of 17 (94%) cyclones in the ascending orbits and only 4 of 9 (45%) cyclones in the descending orbits. As criteria for consideration, the cyclonic center lies within the horizontal boundaries of the satellite swath. Additionally, of the four occurrences observed in the descending data, only two of the differences are displaced greater than 2 degrees. Limited evidence suggests the displacement is related to the strength of the winds in the cyclonic pattern, *i.e.*, moderate to strong wind speed generally have the larger displacements.

The third characteristic difference illustrated in the comparisons encompasses larger displacements.

The third characteristic difference illustrated in the comparisons encompasses

27
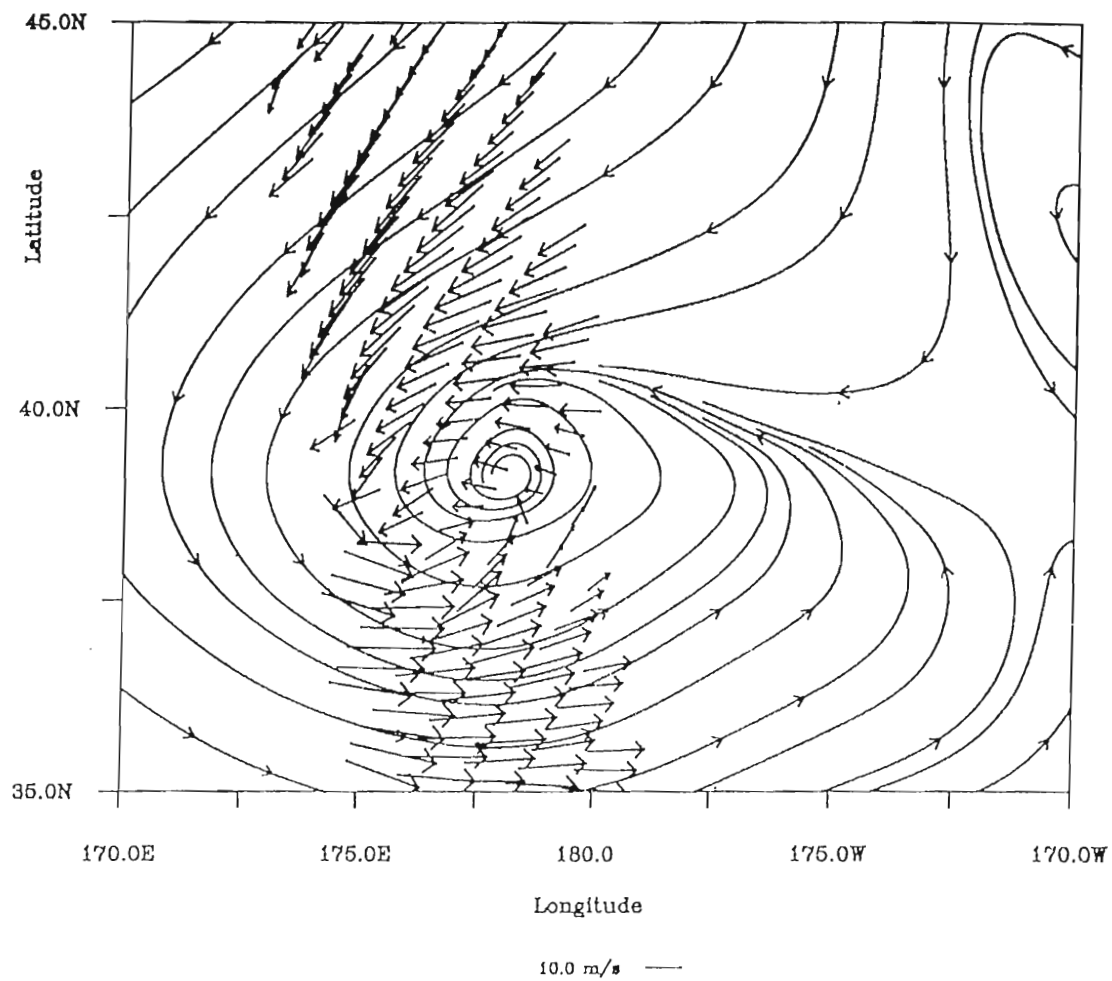
Fig. 5-5: Comparison field, 10Z 18 February 1992. ERS-1 scatterometer derived winds overlaying a stream line analysis of ECMWF/TOGA 10m wind analysis fields interpolated to the same time. ERS-1 overlay illustrates every 5th wind vector.

the structure of the wind speed in coll and cyclonic patterns. The wind speeds of these features are generally stronger in the scatterometer fields. The study finds the scatterometer wind fields do maintain the kinematic structure, *i.e.*, generally decreasing winds progressing towards the center of these features. These results note the scatterometer winds often demonstrate stronger, more distinct curvature in cyclonic flow fields, more asymmetry in the colls, and occasionally, a smaller overall scale for these features, particularly in coll regions. The differences in curvature, scale, and speed are also depicted in a comparison of the vorticity fields computed from the scatterometer and model analysis winds. The limited results indicate the scatterometer derived vorticity fields contain regions of higher absolute vorticity (by as much as +50%) and include increased detail. This characteristic difference likely reflects limitations in ECMWF resolution as well as smoothing of the model analysis. As an aid in illustrating these differences in spatial resolvability, the study notes an 8.5 to 1 numerical superiority in ERS-1 observations to the ECMWF model analysis grid points. Further, these structural differences observed in the wind fields may reflect observational limitations affecting the model analysis during the assimilation process.

Additionally, comparative results highlight wind vector "difficulties" in the ERS-1 wind fields which could be attributed to possible problems with either the C-Band model function or the ambiguity selection scheme. These difficulties generally illustrate an obvious error in the selected ambiguity, *e.g. Fig. 5-6*, and appear to be associated with the difficulty in determining whether the capillary and small gravity waves are traveling toward or away from the sensor. This is often refered to as associated with the difficulty in determining whether the capillary and small gravity waves are traveling toward or away from the sensor. This is often refered to as

29

45.0N

Latitude

40.0N

35.0N

160.0E   165.0E   170.0E   175.0E   180.0

Longitude

10.0 m/s   ———
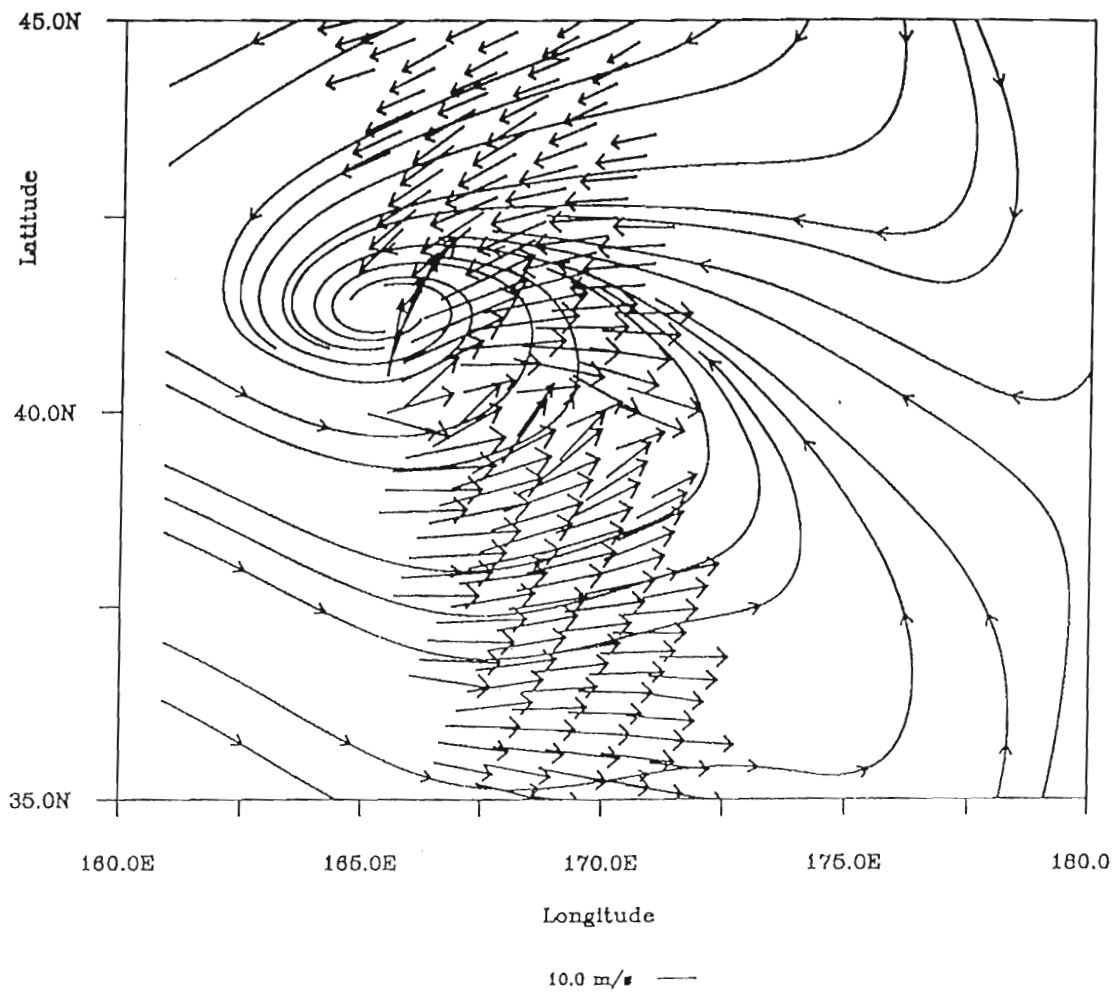
Fig. 5-6: Same as *Fig.* 5-5, for 11Z 17 February 1992.

upwind-downwind symmetry. As discussed by Schulz (1990), the upwind-downwind symmetry is not perfect; σ^o is not the same measuring upwind as measuring downwind. With three or more antennae and in the absence of measurement and modeling error, the maximum likelihood estimate (as described in *Section 2*) would be the true solution.

This study does not attempt to discern the exact nature of observed difficulties in the ERS-1 wind vectors. However, the study results do note a marked improvement with time in comparisons of the ERS-1 wind vectors to ECMWF analyses, and interswath ("nearest neighbor") comparisons. This improvement suggests the σ^o calibrations are a large contributing factor to difficulties with the ERS-1 wind vector ambiguity selection process, particularly during the early portion of the study period.

Difficulties in ambiguity selection are more pronounced in the descending orbits. Both orbit trajectories exhibit erroneous ambiguity selections generally identifiable through interswath ("nearest neighbor") comparisons. Of note, a large number of the erroneous ambiguity selections are located on the north side of cyclonic flow or in broad regions flanked (bordered) on the southern extreme by cyclonic turning of the winds.

5.2 *Monthly and Three Month Mean Comparative Analyses:*

These comparative analyses involve direct comparisons of the monthly and three month means computed from the ECMWF and *in situ* observations to the respective means computed from ERS-1 scatterometer winds. All means represent
and three month means computed from the ECMWF and *in situ* observations to the respective means computed from ERS-1 scatterometer winds. All means represent

31

vector averages and are compared to the climatological results presented by Wright (1988) for representativeness.

In the absence of a reliable assimilation scheme (subjective or objective), the vector averaged COADS individual observations from volunteer observing ships produce unintelligentable patterns for monthly and three month means, *Fig. 5-7* illustrates the three month mean. This results from poor spatial and temporal coverage with each of the three months of COADS data containing approximately 7,000 observations. These poor comparisons serve to strengthen the usefulness of remotely sensed winds.

The qualitative results from comparisons of ECMWF monthly and three month means to the corresponding scatterometer means demonstrate poor agreement between the data sets for the month of January with the magnitudes of the scatterometer winds generally stronger and directional correspondence providing only vague agreement. As mentioned previously, January scatterometer data are scarce with a substantial period of missing observations. The limited number of observations and the changing σ^o calibrations account for a large portion of the discrepancy. The two data sets demonstrate a greater correspondence during the months of February and March, improving over the period. This improvement reflects the increased scatterometer observations and possibly the effects of improved calibration and/or less monthly variability as compared to the month of January; hence making it easier to correlate the two wind fields . The larger number of scatterometer observations serve to increase the statistical viability of the resultant mean wind field. The three month mean the two wind fields . The larger number of scatterometer observations serve to increase the statistical viability of the resultant mean wind field. The three month mean

32
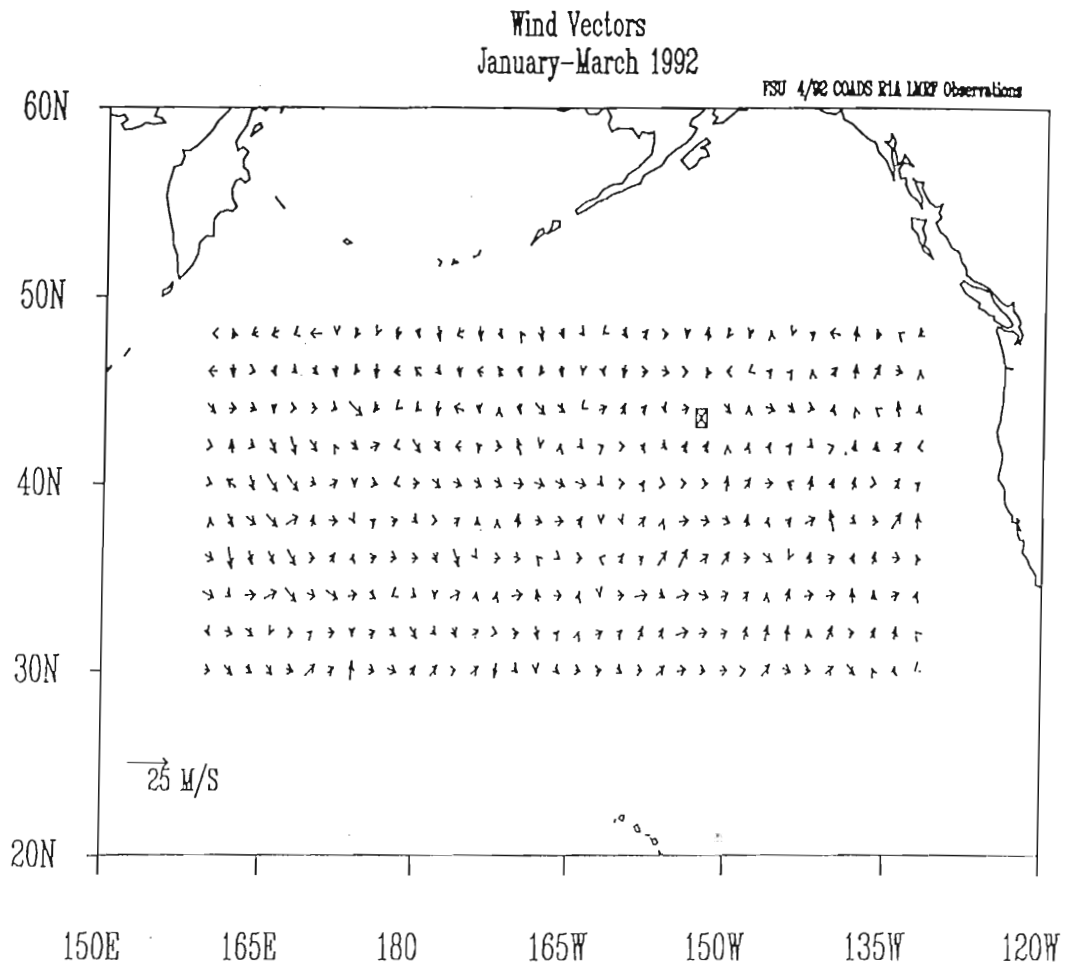
Fig. 5-7: Three month, vector averaged mean of all COADS observations from January - March 1992 binned to 1.125° by 1.125° boxes. A boxed "x" indicates no observations were available.

demonstrates good agreement with the ECMWF mean and climatology. The rms differences for the three month mean wind field computed in the study compare favorably with the results presented by Halpern *et al.* (1992). The monthly and three month means computed from the scatterometer data represent the mean wind field removed from the original data prior to the EOF analysis, hence, only the data locations containing 18 or more observations over the study period were used in these comparisons, *Figs. 5-8, 5-9 and 5-10.*

The rms differences between the scatterometer and ECMWF mean wind fields were computed separately for each orbit trajectory using coincident grid locations (nearest ERS-1 wind vector within 13 km of the ECMWF comparison wind vector) and an arithmetic average of the coincident and "nearest neighbors" (all ERS-1 wind vectors within 37 km of the comparison ECMWF wind vector), TABLE 5-1.

TABLE 5-1: Comparative rms results of ECMWF and ERS-1 mean wind fields. Coincident indicates a calculation using ECMWF wind vectors with the nearest scatterometer wind vector within 13 km and areal averages indicate calculation is based on the mean of all ERS-1 vectors within 37 km of ECMWF grid value.

	WIND SPEED			
	Coincident Grid Points		Areal Average	
	Ascending	Descending	Ascending	Descending
January	3.48 ms^{-1}	2.78	3.16 ms^{-1}	2.46
February	2.30	2.18	2.11	2.15
March	2.17	1.52	2.02	1.54
Jan-Mar	1.36	1.11	1.28	0.97

	WIND DIRECTION			
	Coincident Grid Points		Areal Average	
	Ascending	Descending	Ascending	Descending
an-Mar	17.4°	22.3	16.8°	22.4
	Coincident Grid Points		Areal Average	
	Ascending	Descending	Ascending	Descending
an-Mar	17.4°	22.3	16.8°	22.4
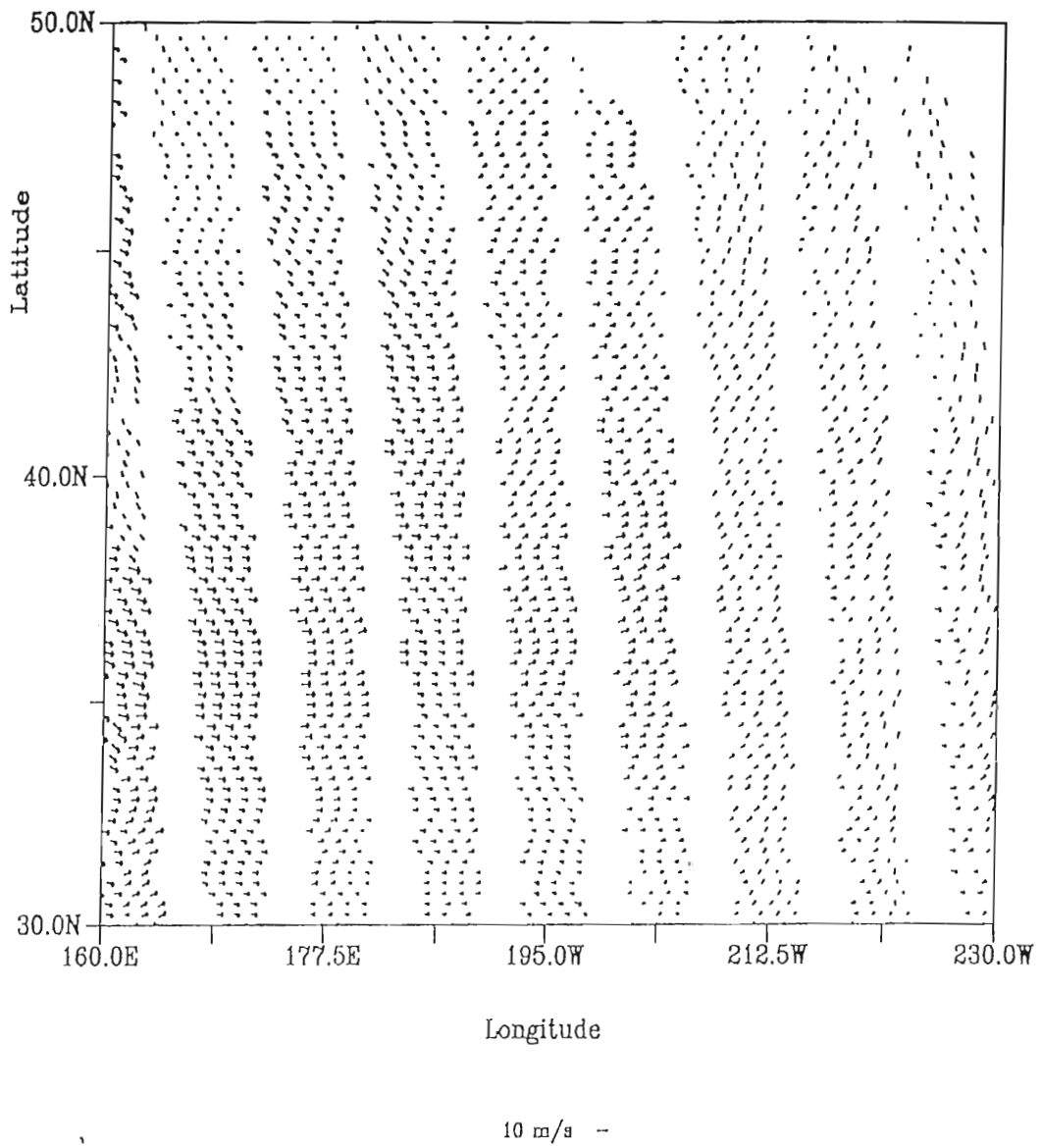
Fig. 5-8: Three month, vector averaged mean of ascending scatterometer data used in the EOF analysis. Every 5th vector plotted.

35
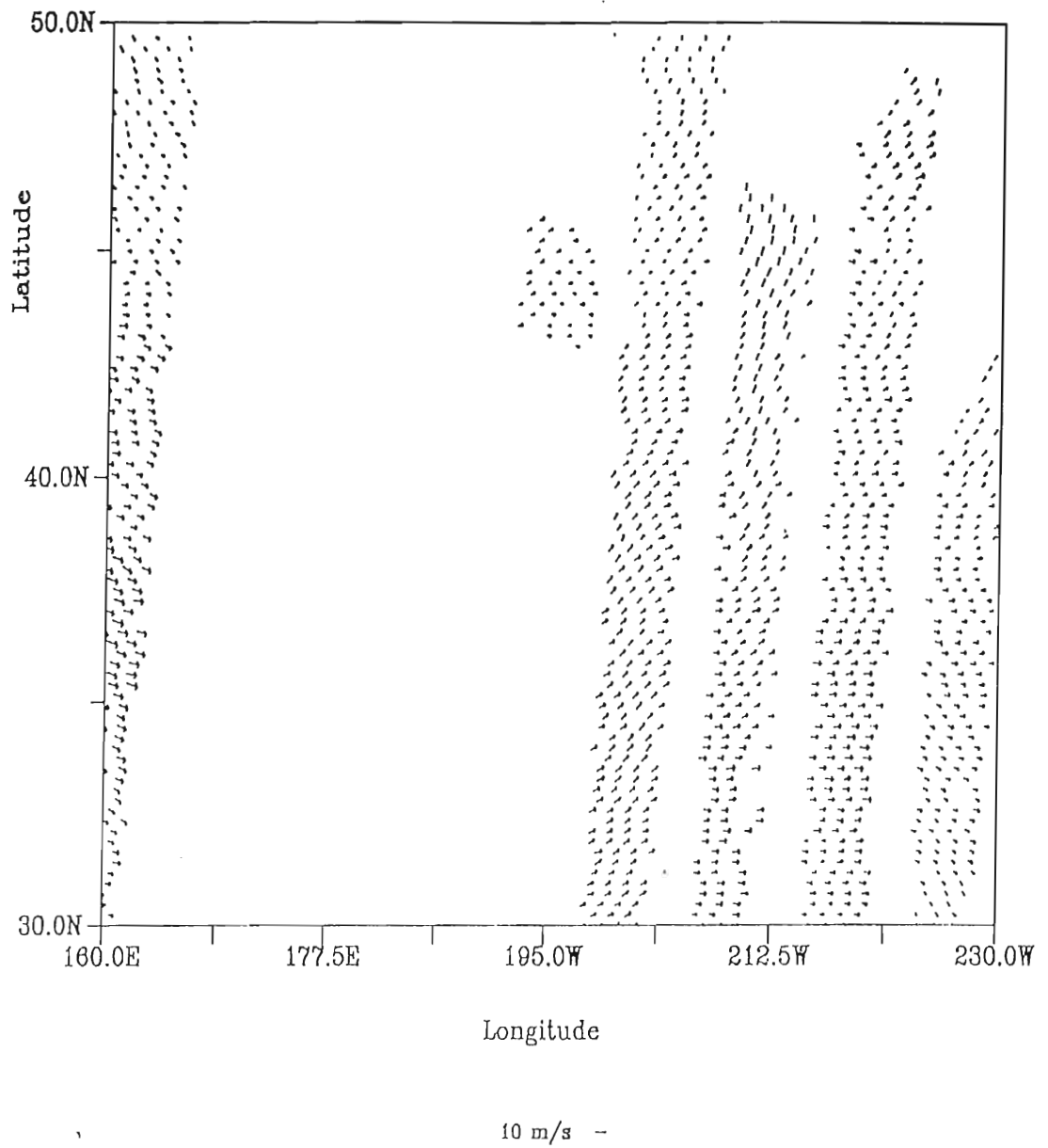
Fig. 5-9: Three month, vector averaged mean of descending scatterometer data used in the EOF analysis. Every 5th vector plotted.
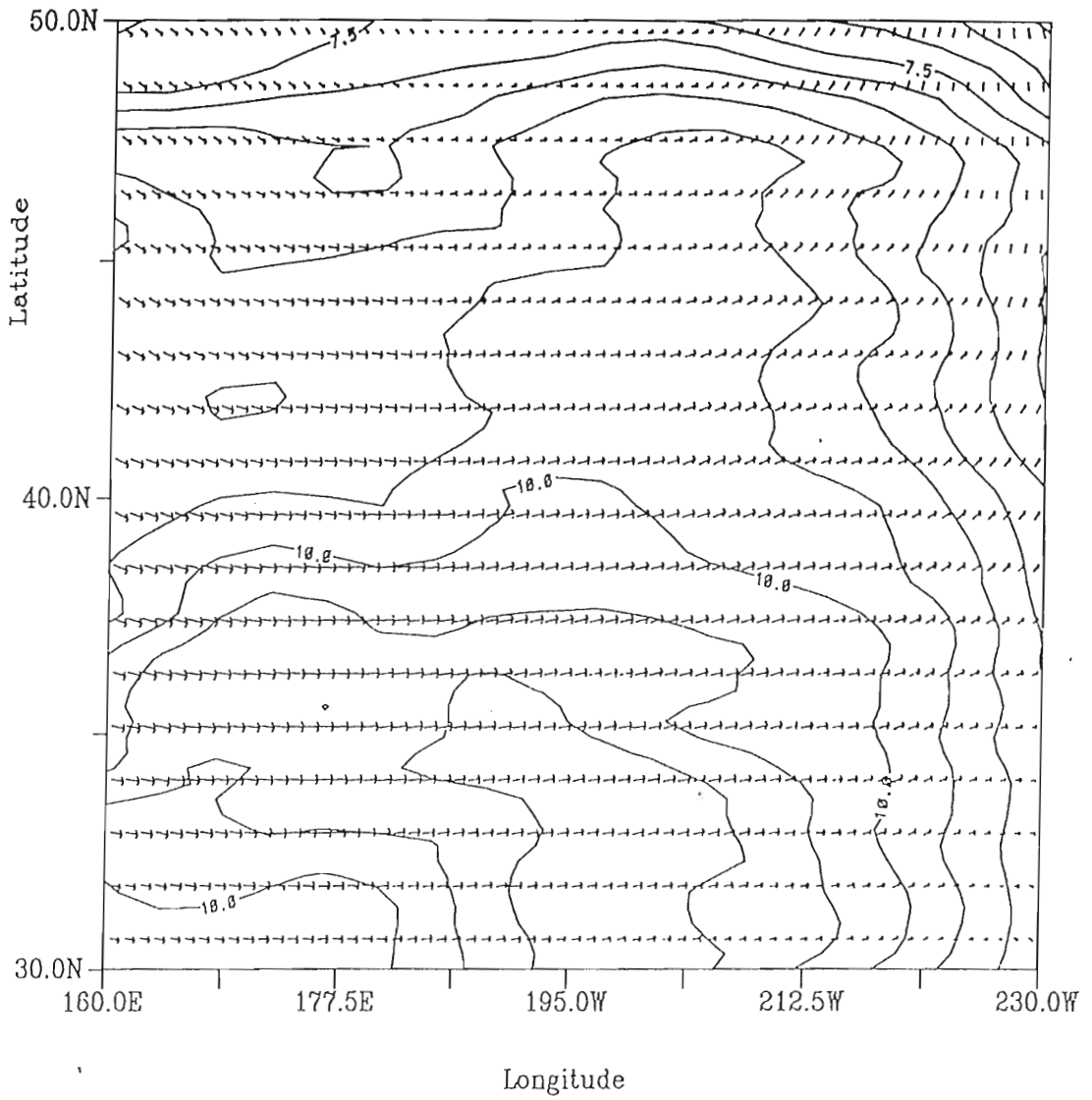
Fig. 5-10: Three month, vector averaged mean of ECMWF/TOGA model analysis.

As expected, these results show improvement in the rms differences of wind speed through the study period in both data sets. Based on uncertainties in interpreting rms differences of direction, only the three month rms value for direction is presented noting the individual months exhibited a wide range of rms directional values. Both trajectories highlight the poor January data availability. Further, the results illustrate smaller rms differences between the descending data and the ECMWF analysis fields. As discussed previously, the bulk of the descending scatterometer observations are confined to the southeastern portion of the study region. Climatology indicates the winds in this area are generally weaker than the winds in the remaining portion of the study region due to the influence of a weak subtropical high pressure system.

5.3 *Description of Physically-Motivated Phenomena:*

The first few EOFs and associated spatial patterns illustrate a partitioning of the energy or variance into periodic or oscillatory structures. The first four eigenvectors for both the ascending and descending data account for 50% or more of the total variance sampled in the wind data, TABLE 5-2. As discussed previously, the descending data array is limited in coverage, *Fig. 3-2*. The absence of observations in the western half of the study region drastically limits the variability sampled by the descending data, therefore, differences between the ascending and descending data EOFs are expected. The limited data also provide an interesting opportunity to compare and contrast regional contributions to the total variance evident in the study EOFs are expected. The limited data also provide an interesting opportunity to compare and contrast regional contributions to the total variance evident in the study region as a whole.

38

TABLE 5-2: Variance accounted for by the eigenvectors.

Eigenvector	Ascending		Descending	
	(%)	Cumulative Total (%)	(%)	Cumulative Total (%)
E_1	19.0	19.0	25.3	25.3
E_2	12.6	31.6	15.1	40.4
E_3	9.7	41.3	10.2	50.6
E_4	8.7	50.0	9.5	60.1
E_5	7.0	57.0	6.5	66.6
E_6	5.8	62.8	5.5	72.1
E_7	4.8	67.6	3.9	76.0
E_8	4.4	72.0	3.7	79.7
E_9	4.0	76.0	*Within the level of noise*	

Based on climatology (Barry *et al.*, 1982 and Wright, 1988), the seasonal variability in the winds is strongest in the western and northern sections of the study region. Further, the inter-seasonal variability associated with storm systems is strongest during the northern hemisphere winter in these same areas. The southeastern section of the study region remains under the influence of a subtropical high pressure system throughout the year. The strength of this system is weakest during the northern hemisphere winter (study period). The structure of the mean winds, discussed in *Section 2*, highlight this variability in the stronger mean wind speeds prevalent throughout the western region. Both the ERS-1 (ascending orbits) and ECMWF winds reflect this structure.

Though not an area prone to frequent storm systems, the southeastern area does include secondary storm tracks (Barry *et al.*, 1982) defined by the limited, but
Though not an area prone to frequent storm systems, the southeastern area
include secondary storm tracks (Barry *et al.*, 1982) defined by the limited, but decernable, frequency of low pressure systems migrating through the area. With the

eastern portion of the study region under the influence of a weak subtropical high pressure cell, the secondary storm tracks (generally associated with individual storms rather than complex systems) are a strong source of variability in the descending data. In the case of the ascending orbits, the contributions of the complex general circulation systems (vigorous low pressure system(s) and associated strong frontal activity) outweigh the contributions of the individual storm systems that may make up the more complex structure.

The study explores the results of the EOF analysis to decern the possibility and subsequent description of physically-motivated phenomena attributed to the EOF and associated spatial patterns. The study examines the individual time series, evaluating the amplitude and phase combination for definable periodicities. The limited number of points (30) in the complex time series (EOFs) prevent the application of a robust spectral analysis. Despite the limitations, the study utilizes a simple spectral analysis of the first four significant EOFs in an attempt to descern periodicities. As expected the results depict a large amount of "red noise". Of note, the spectral analysis of the first EOF does produce a strong, definable harmonic with a period of 22 days but beyond this, the spectral analysis does not clearly illustrate definable periodicities.

Additionally, the study examines the spatial patterns for definable structures. These spatial fields are reviewed separately and when modulated by the associated time series. In the latter case, the EOF/Spatial pair produce a reconstructed wind field representing a small portion of the total variability sampled in the data (TABLE 5-2). Computer animation illustrates the details of the time series modulation and provides representing a small portion of the total variability sampled in the data (TABLE 5-2). Computer animation illustrates the details of the time series modulation and provides

greater flexibility in decerning possible atmospheric features.

The study results suggest the first EOF and associated spatial field for both the ascending and descending data portray the long wave or planetary wave pattern. Analysis of the ascending and descending time series (*Figs. 5-11 and 5-12*) depicts periodicities of 18-21 days. The spatial field for the ascending data suggests a length scale of approximately 5000 km roughly describing a planetary wave number of 5, *Fig. 5-13*. This pattern is likely to be combined with other patterns (EOFs), in effect, modulating the long wave pattern. Based on the phase of the temporal component, this spatial field exhibits an oscillatory nature fluctuating between a trough and ridge feature. A reconstruction of the wind fields using just the first EOF information validates this oscillatory motion and pattern. These results follow the descriptions presented by Carlson (1991) in describing the wavelength and growth rate of baroclinic waves.

For the second EOF, the study results suggest regional differences between the ascending and descending data sets. Based on the discussions presented in Sections 2 and 3, these regional differences are expected. Examination of the individual time series (*Figs. 5-14 and 5-15*) highlights definable harmonics, approximately 10 and 7 days for the ascending and descending data sets, respectively. Both spatial fields include recognizable anti-cyclonic flow patterns (*Figs. 5-16 and 5-17*). When modulated by the associated time series, these regions depict cyclonic and anti-cyclonic flow fields. Further, the spatial fields suggest length scales for these patterns of 2000-2500 km in the ascending data and 1200-1800 in the descending data. The cyclonic flow fields. Further, the spatial fields suggest length scales for these patterns of 2000-2500 km in the ascending data and 1200-1800 in the descending data. The

41

a)
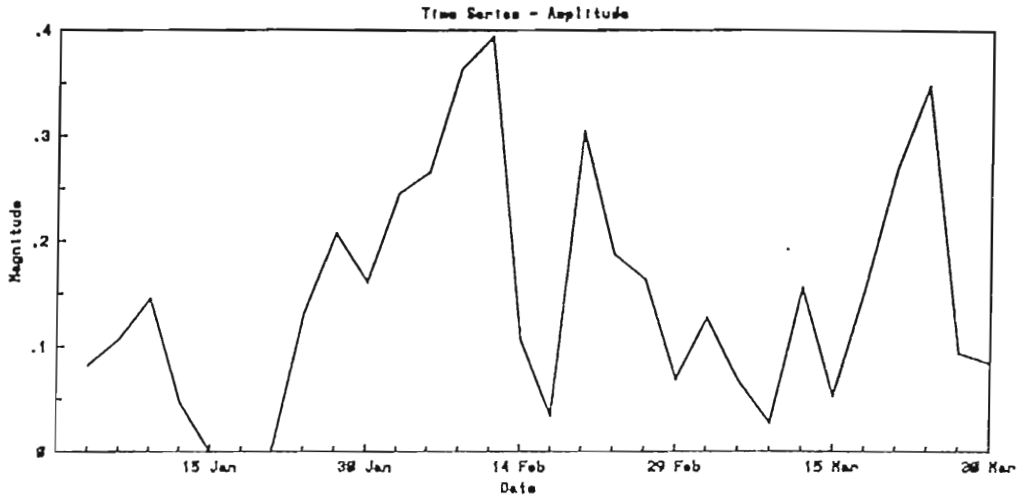
b)
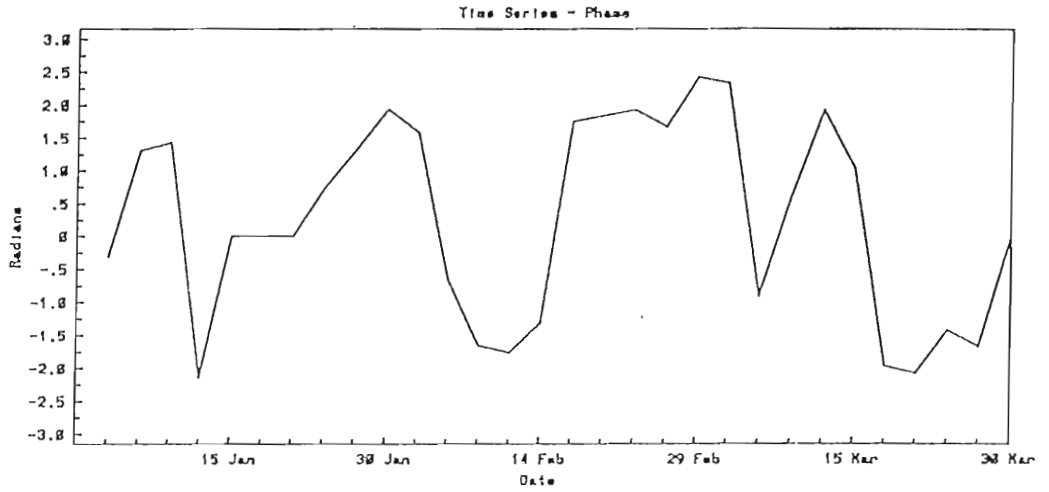
Fig. 5-11: 1st ascending EOF, complex time series illustrating a) the magnitude and b) the phase, negative phase indicates clockwise turning of the individual vectors of the spatial field.

42

a)
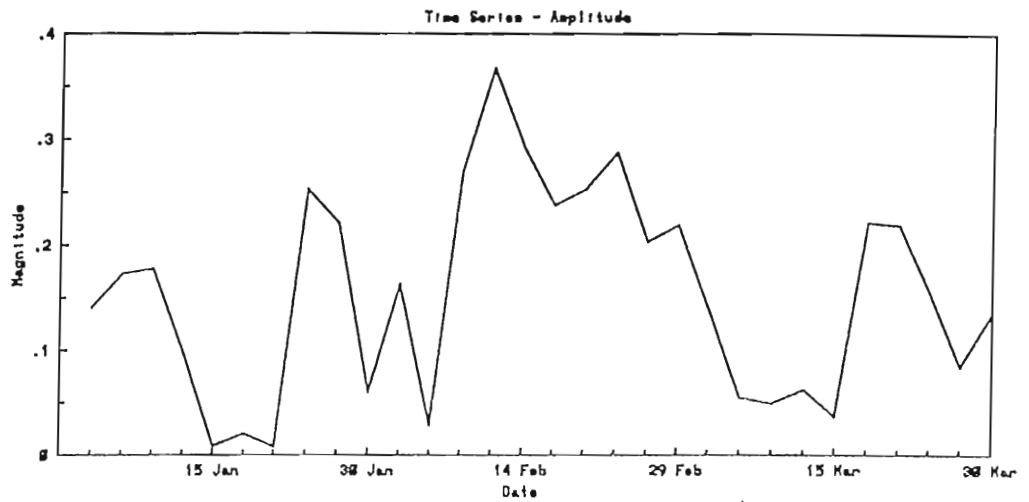
b)
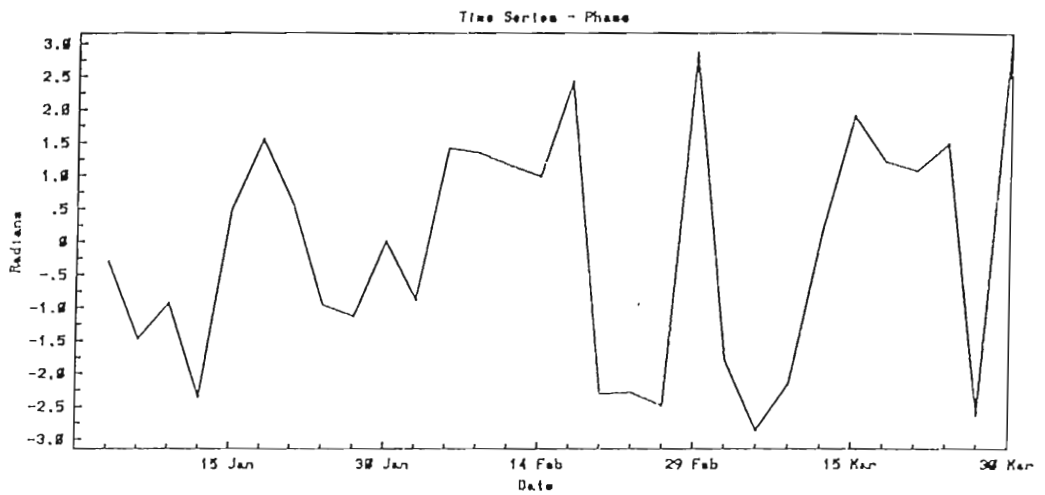
Fig. 5-12: 1ˢᵗ descending EOF, complex time series illustrating a) the magnitude and b) the phase, negative phase indicates clockwise turning of the individual vectors of the spatial field.
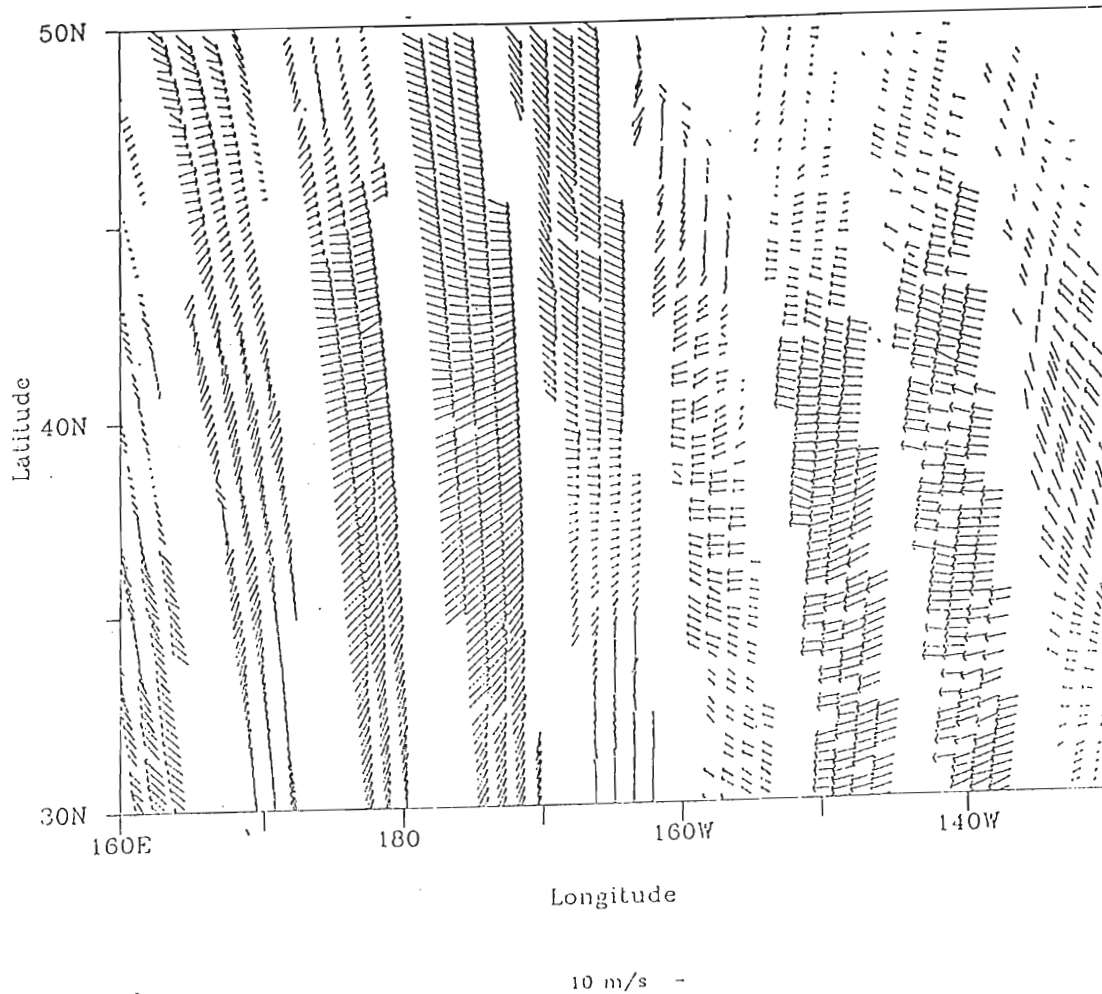
Fig. 5-13: 1ˢᵗ EOF ascending spatial field.

a)
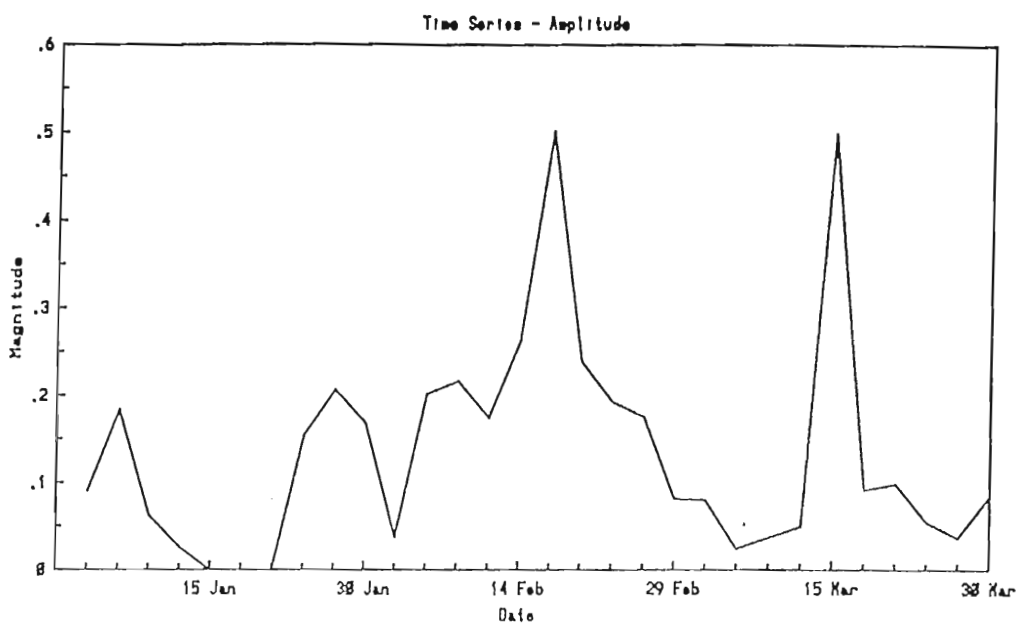
b)
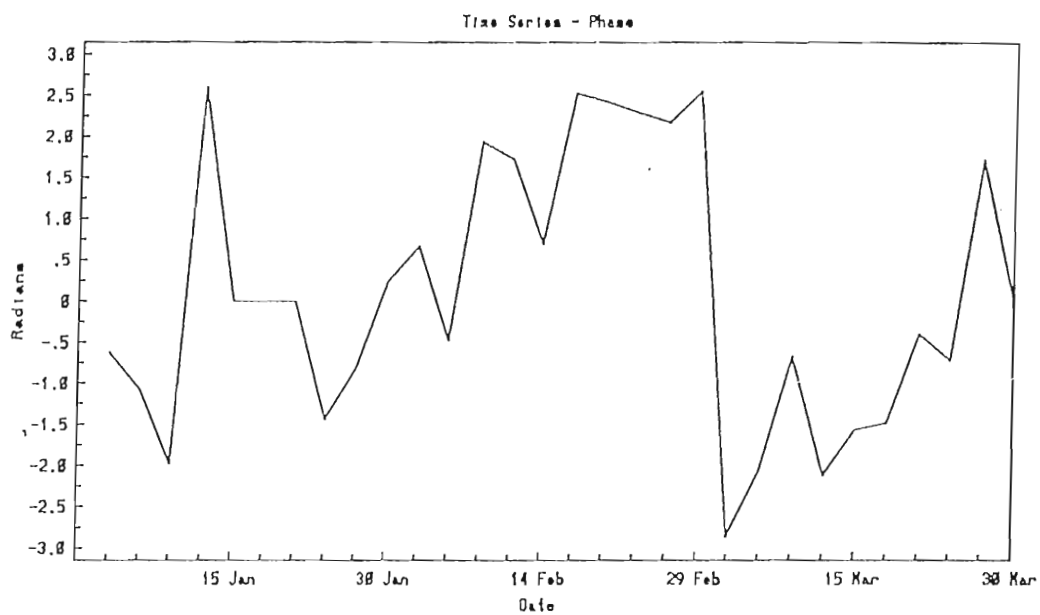
Fig. 5-14: Same as *Fig. 5-11* for 2nd EOF.

Fig. 5-14: Same as *Fig. 5-11* for 2nd EOF.

a)
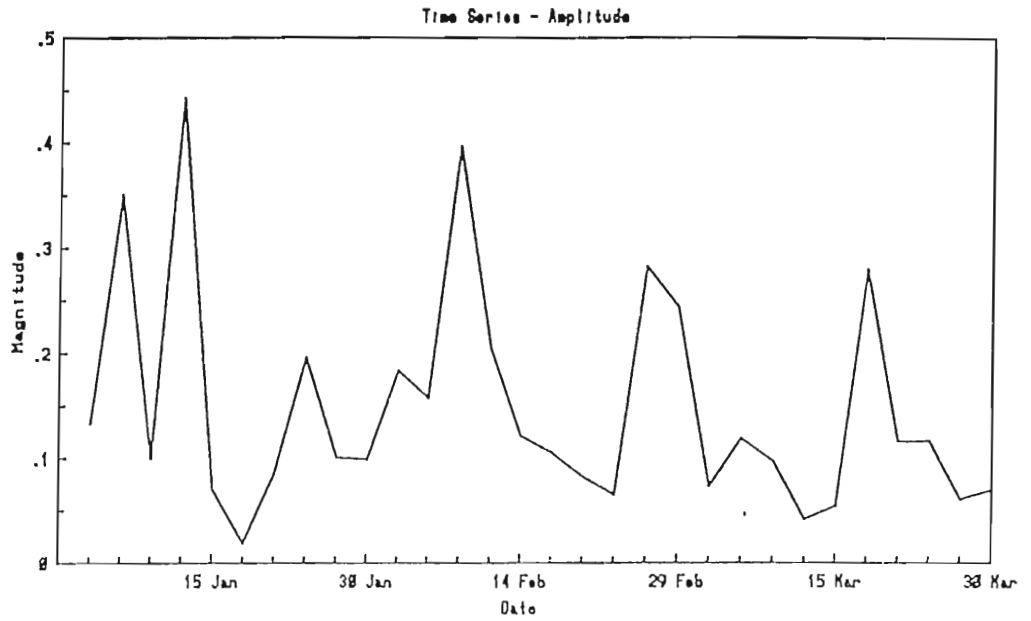
b)
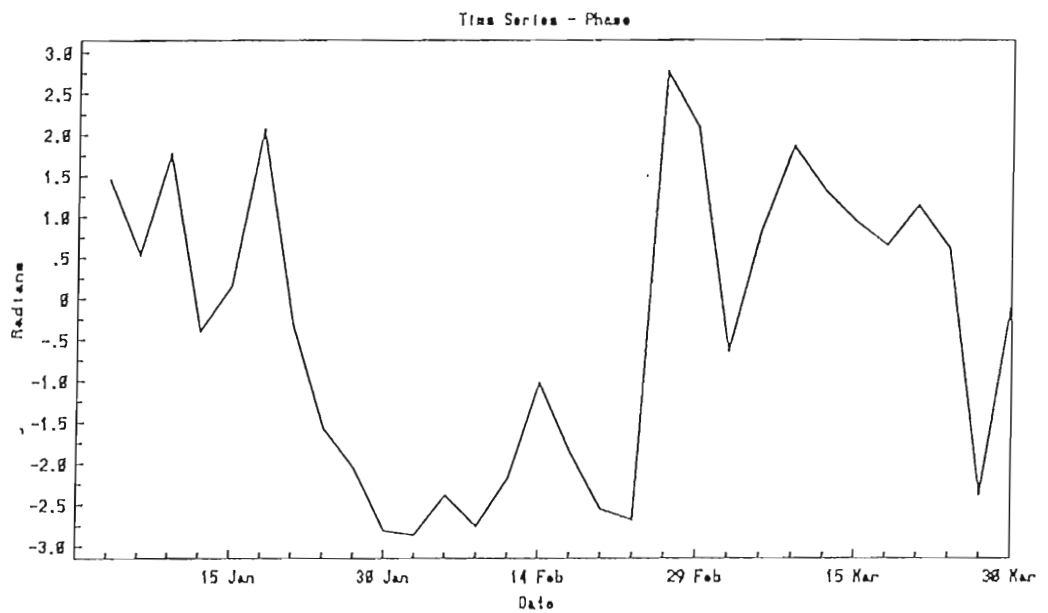
Fig. 5-15: Same as *Fig. 5-12* for 2nd EOF.
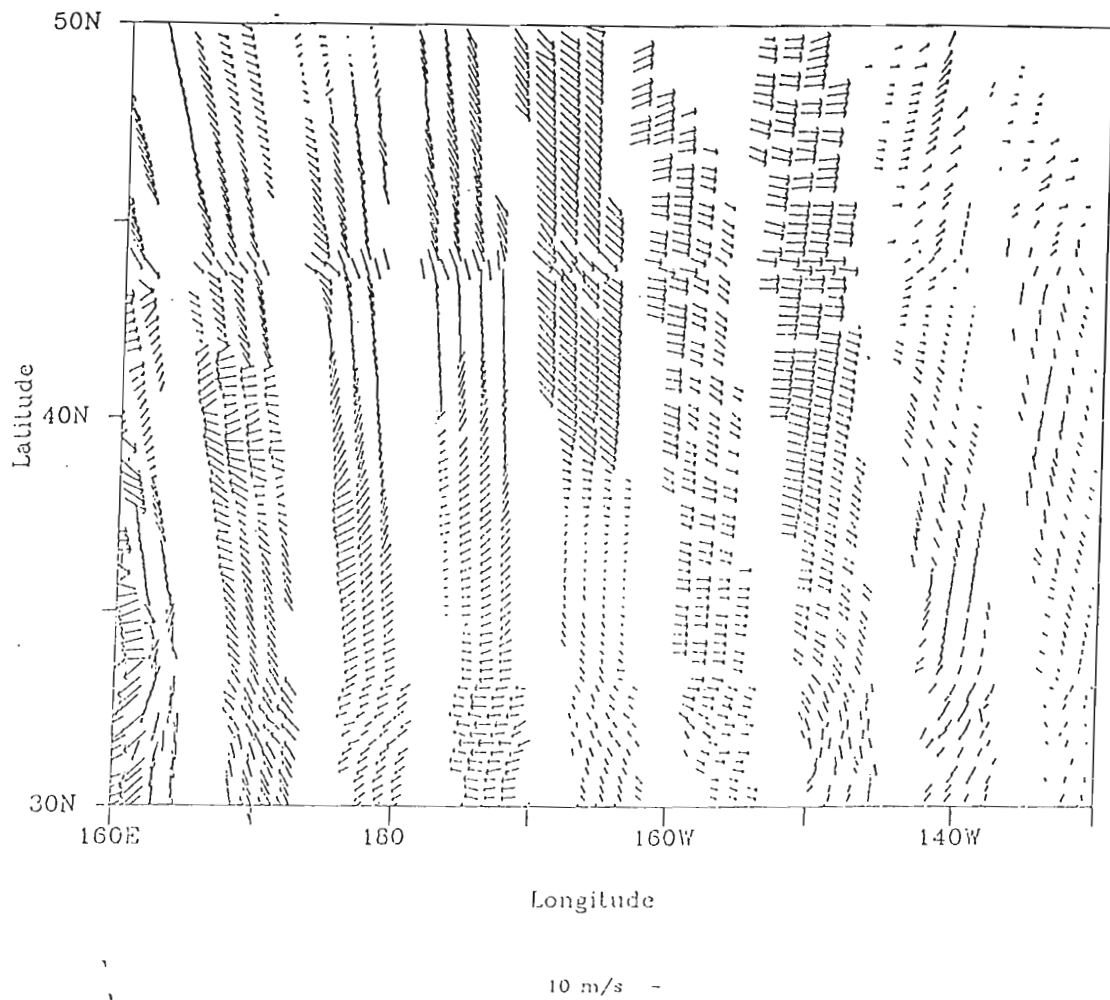
Fig. 5-16: 2st EOF ascending spatial field.
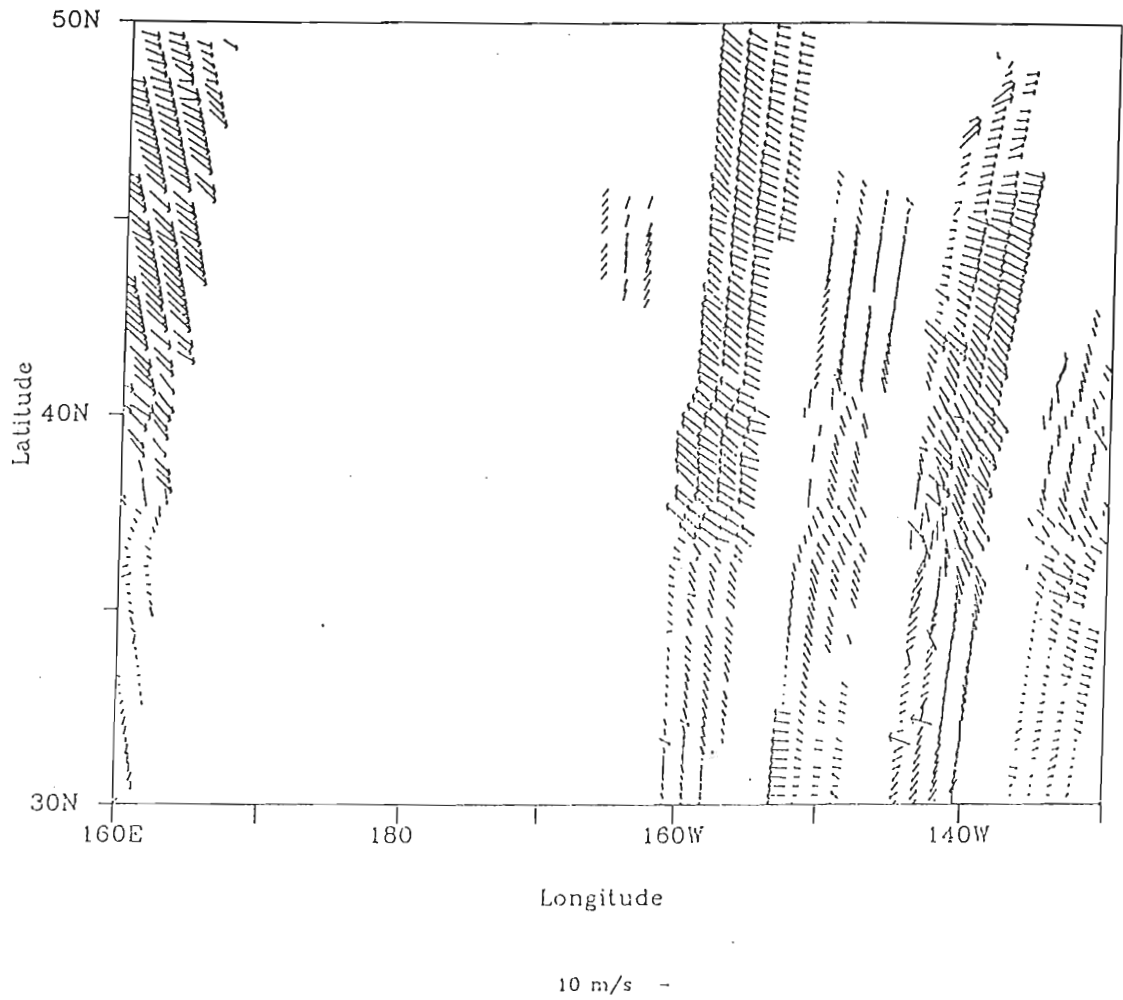
Fig. 5-17: 2st EOF descending spatial field.

computer animation of the modulated spatial fields resemble large general circulation patterns in the western portion of the ascending data and smaller scale cyclonic activity in eastern section of the descending data.

The third and fourth EOFs, individually account for a sizeable contribution to the total variance sampled in each data set (9-10% each). Examination of the individual time series depicts periodicities of 7-10 days. The associated spatial patterns include smaller scale cyclonic and anti-cyclonic flow fields with smaller associated length scales of 700 - 2000 km. Results of the computer animation suggest these features depict smaller scale cyclonic activity.

The remaining EOFs for both the ascending and descending data sets add increasing detail to cyclonic patterns and further modulate, "correct", or are additive terms to the previous spatial fields. These EOFs often incorporate multiple frequencies and complex spatial patterns defying simplistic interpretations. This study does not attempt to attribute physically-motivated phenomena to these remaining EOFs and spatial fields. Adding these spatial and temporal components to the first four EOFs adds increasing complexity to the wind fields. As presented in the proceeding subsection, incorporating the EOFs through the first 8 to 9 accounts for approximately 80% of the variability sampled in the original data field.

In short, the EOF technique demonstrates a partitioning of the variance into spatial/temporal "bands". The study results suggest periods of 18-21 days, 8-10 days, and 6-8 days. These reflect the expected time scales associated with the planetary wave cycle, large scale general circulation systems, and smaller scale storm structures; and 6-8 days. These reflect the expected time scales associated with the planetary wave cycle, large scale general circulation systems, and smaller scale storm structures;

respectively (Barry *et al.*, 1987 and Carlson, 1991). The first four EOFs, those for which the results suggest physically motivated phenomena, account for 50-60% of the total variance sampled in the data. As a matter of interest, the partitioning of the variance can be used to evaluate the filtering aspects of the analysis technique in extracting information above the level of noise in an EOF reconstruction of the wind fields.

5.4 *EOF Reconstruction of the Scatterometer Fields:*

In evaluating the physically-motivated phenomena associated with the first few EOFs, the study also evaluates the filtering aspect of the EOF technique as a means for removing noise and erroneous wind vector ambiguities. The study utilizes a Monte Carlo simulation method to determine the significant EOFs. This follows the PCA statistical discussions presented by Preisendorfer (1988). The study finds the first 9 ascending and first 8 descending EOFs to be statistically significant, TABLE 5-3. Individual EOFs beyond these can be considered within or below the level of noise. The study conducted 100 simulations for each β to develop the statistical limits. These statistical limits compare favorably with the results of asymptotic theory presented by Preisendorfer (1988) and provide a major extension to his results (his results list only through $\beta=100$).

The study produces four reconstructed wind fields using first all 30, then the first 8 (or 9 for ascending wind fields), 6, and 4 EOFs and spatial fields for numerous

first 8 (or 9 for ascending wind fields), 6, and 4 EOFs and spatial fields for numerous small areas (5° Lat by 10° Long to provide greater detail) throughout the study period.

The study actually applies this technique to the entire analysis region, but a focus on a small area provides a clearer evaluation of the results (*Figs. 5-18 through 5-21 exemplify the tests*).

TABLE 5-3: Average eigenvalues, x (presented as the percentage contribution to the total variance), for covariance matrices generated from random data. $P(x,\beta)$ is the percentage of remaining average eigenvalues, x, contributing less to the total variance sampled in the random data. β represents the order of the data matrices, number of rows divided by the number columns.

$P(x,\beta)$	100.00	90.00	80.00	70.00	60.00	50.00	40.00	30.00	20.00	10.00
β=450	3.63	3.53	3.46	3.41	3.37	3.32	3.28	3.24	3.18	3.12
400	3.63	3.54	3.46	3.41	3.37	3.32	3.28	3.24	3.18	3.11
350	3.68	3.56	3.48	3.42	3.37	3.33	3.28	3.23	3.16	3.09
300	3.70	3.58	3.49	3.42	3.37	3.32	3.27	3.22	3.15	3.07
250	3.73	3.60	3.50	3.44	3.37	3.32	3.26	3.20	3.14	3.05
200	3.76	3.62	3.52	3.45	3.38	3.32	3.26	3.19	3.12	3.02
150	3.88	3.69	3.56	3.47	3.38	3.31	3.23	3.16	3.07	2.97
100	3.96	3.75	3.60	3.50	3.40	3.31	3.22	3.12	3.02	2.89
75	4.10	3.83	3.63	3.51	3.40	3.29	3.19	3.10	2.98	2.83
50	4.30	3.94	3.71	3.55	3.40	3.28	3.15	3.03	2.89	2.72

Reconstruction of the wind fields using only the first 4-6 EOFs, significantly reduces the magnitude and directional error of the inaccurate wind vectors. The success of this level of filtering is generally related to the type of ambiguity error (upwind-downwind symmetry or other) and the number of erroneous ambiguities located in the area. Isolated, erroneous wind vectors not associated with upwind-downwind symmetry are effectively removed in this level of filtering. Conversely, numerous erroneous wind vectors or ambiguity errors associated with upwind-downwind symmetry (a large area of erroneous wind vectors are often, but not always, numerous erroneous wind vectors or ambiguity errors associated with upwind-downwind symmetry (a large area of erroneous wind vectors are often, but not always,

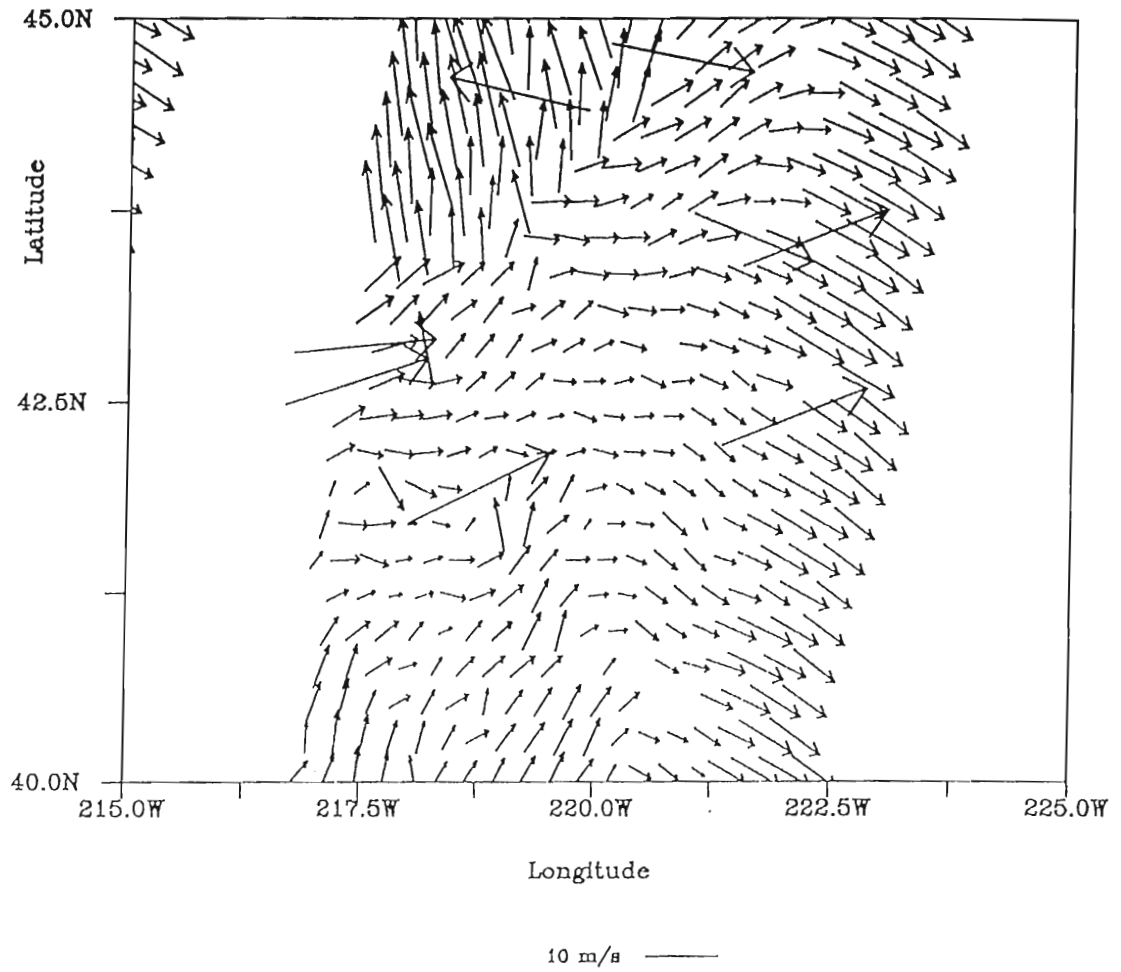*Fig. 5-18*: EOF reconstruction of a descending wind field (9 January 1992) using all 30 EOFs. All wind vectors are plotted.
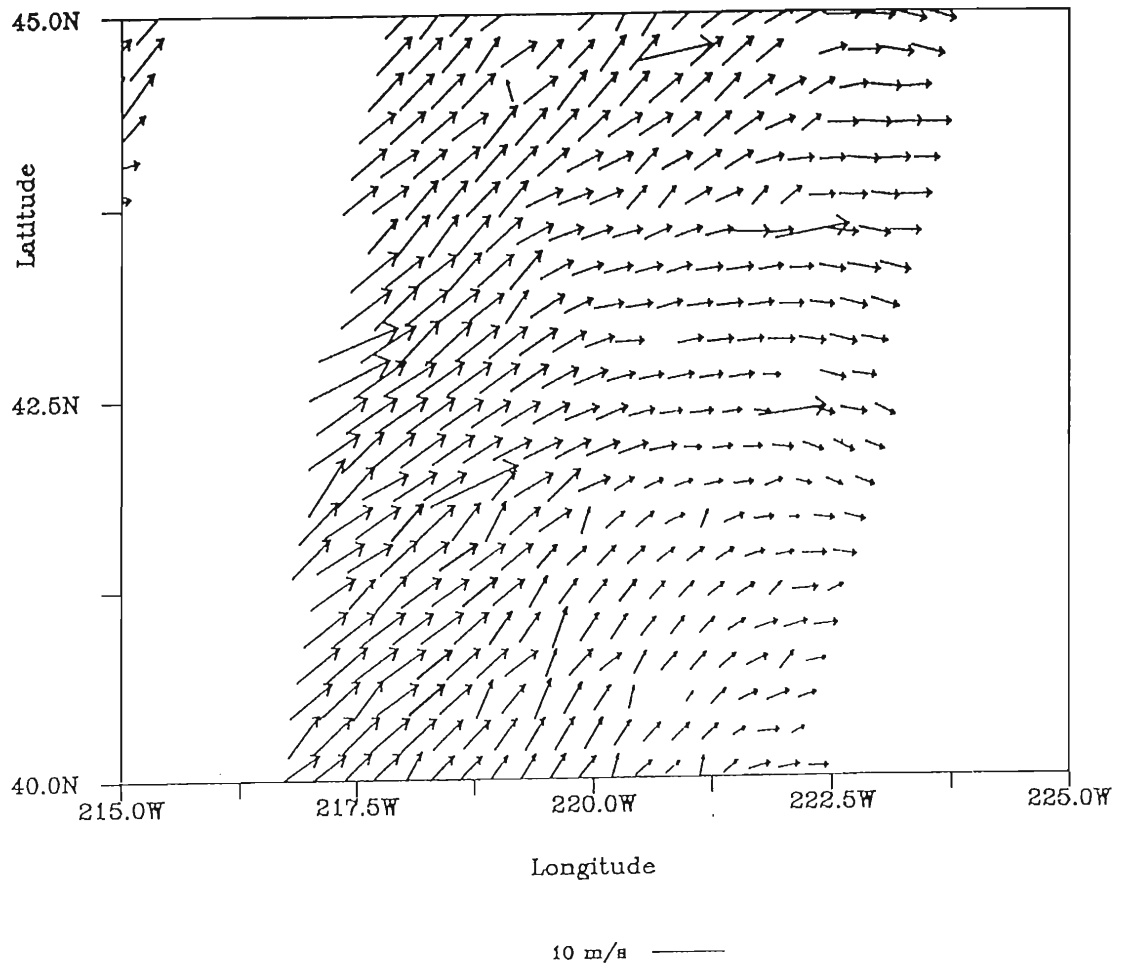
45.0N

Latitude

42.5N

40.0N

215.0W   217.5W   220.0W   222.5W   225.0W

Longitude

10 m/s ——

Fig. 5-19: Same as *Fig. 5-18* using 8 EOFs.
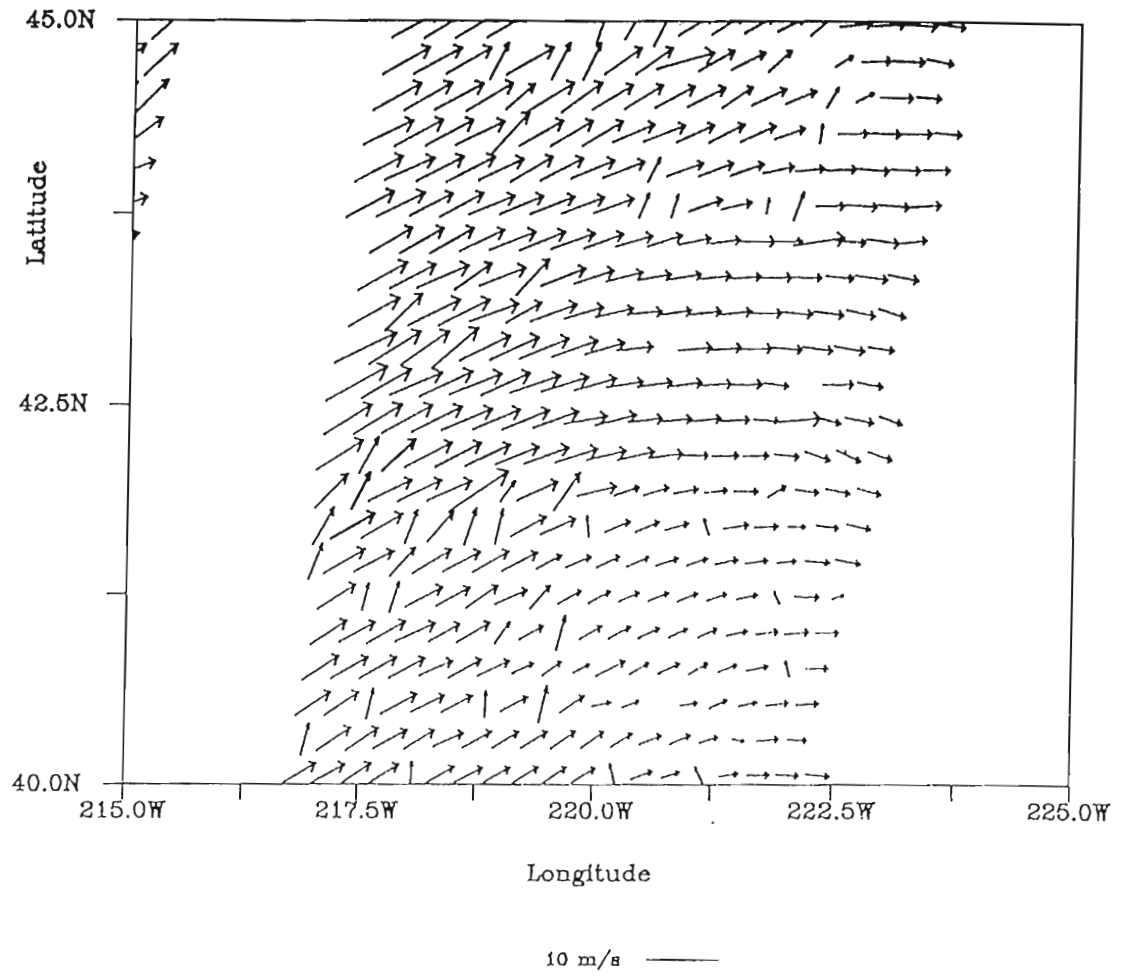
Fig. 5-20: Same as Fig. 5-18 using 6 EOFs.
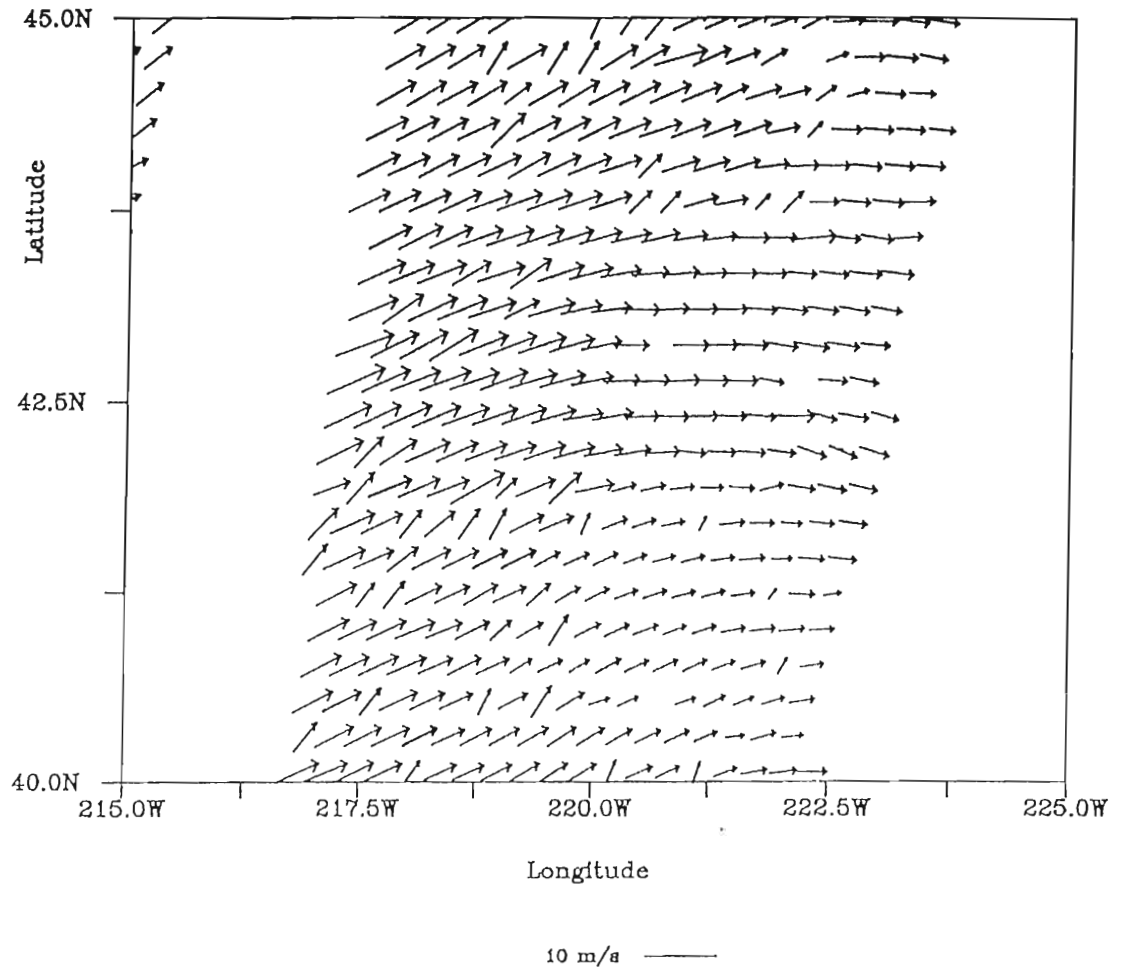
Fig. 5-21: Same as *Fig. 5-18* using 4 EOFs.

55

associated with upwind-downwind symmetry problems) are only moderately affected by this level of filtering. The filtering capabilities using only the significant EOFs (the first 8 in the descending and 9 in ascending data) are, at best, limited. The incorrect ambiguities appear to undergo a 30-50% reduction in magnitude generally accompanied with a directional change of 10-40 degrees. This is generally inadequate in eliminating upwind-downwind symmetry errors.

As noted previously, the first 4-6 EOFs account for 50-63% and 60-72% of the total variance in the ascending and descending data, respectively. The reconstructed wind fields from the EOFs provide a good evaluation of the mean wind field over the three month period due to the retention of the dominant long-scale features and the elimination of the smaller scale weaker features lost in or below the level of noise. In general, 4-6 EOFs maintain most of the kinematic structure but with weaker winds and less curvature. These resultant wind fields reflect the smooth large scale structures of the atmosphere.

For greater detail, the study uses all the significant EOFs (8 and 9 for the descending and ascending data fields; respectively) to generate wind fields which account for approximately 76-80% of the total variance. These reconstructed fields generally maintain the original spatial level of detail with only a slight reduction in magnitudes on the order of 5-10%. The filtering aspects of using all the significant EOFs provide characteristically poor erroneous wind vector deletion/correction.

The most pronounced aspect associated with EOF wind field reconstruction lies

The most pronounced aspect associated with EOF wind field reconstruction lies in the possibilities associated with ambiguity selection. As discussed previously, the

wind vector retrieval algorithm involves the C-Band model function and the ambiguity selection scheme. As noted by Schultz (1990), model and/or instrument error may allow for an alias as the solution with the greatest likelihood estimate. This study notes, with a brief exception during the second week of January, the bulk (80-90%) of the erroneous ambiguity selections appear to be associated with the upwind-downwind symmetry problem. An EOF analysis from an independent data source (*i.e.*, training data set, *e.g.* the ECMWF analyses used in this test), could be used to select the correct ambiguity. Of note, an atmospheric general circulation model (AGCM) analysis fields are used in the formulation of the C-Band model function but not in the ambiguity selection scheme. Further, the proposed EOF technique would represent a correction for upwind-downwind symmetry problems only.

5.5 *Combined Three Day Fields:*

An underlying objective of this study is to examine the possibility of combining the ascending and descending data fields into one synthesized three day field. The intent of the combined field is to encompass as much of the information content exhibited in the ascending and descending scatterometer fields as possible. The original premise for separating the scatterometer data by orbit trajectory is to avoid the problems associated with averaging wind vectors separated by more than 12 hours while maintaining the three day variability. Using the EOF analysis technique to partition the variance, two wind vectors, one from the ascending and descending

partition the variance, two wind vectors, one from the ascending and descending orbits, reconstructed from a limited number of EOFs can be combined without

seriously degrading the information content. As discussed previously, the first few EOFs of both orbit types share similar physical interpretations, thus the ascending and descending EOF pairs depict approximately the same spectral band making it more likely that a combination of the two will lead to improved wind fields. The study combines ascending and descending data reconstructed from the significant EOFs for each orbit type with a vector average of the two reconstructed fields. The study evaluates two other methods for combining the ascending and descending fields but eliminates these from consideration due to the poor attributes of or the "zero sum gain" in spatial coverage resulting from the synthesized field.

The first method involves projecting the ascending EOFs onto the descending data. The technique assumes the ascending EOFs are representative of the region as a whole and serve to accent, in the descending data, the spatial scales exhibited in the ascending spatial fields. The resultant synthesized three day field resembles the simple vector average method with a slight loss of detail. The second technique is the construction of the synthesized field through the use of a combined complex time series (ascent plus descent) to modulate the ascending spatial field. This technique assumes the ascending spatial fields are representative of the region as a whole. This method does not increase the spatial coverage, hence "zero sum gain".

The combination of the ascending and descending EOF reconstructed data effectively increases the coverage over the study region, *Fig. 5-22*. The total three day coverage fills in many of the gaps found in the eastern section of the study region. In the absence of missing data, only small areas (primarily centered on 38 degrees north

10 m/s –
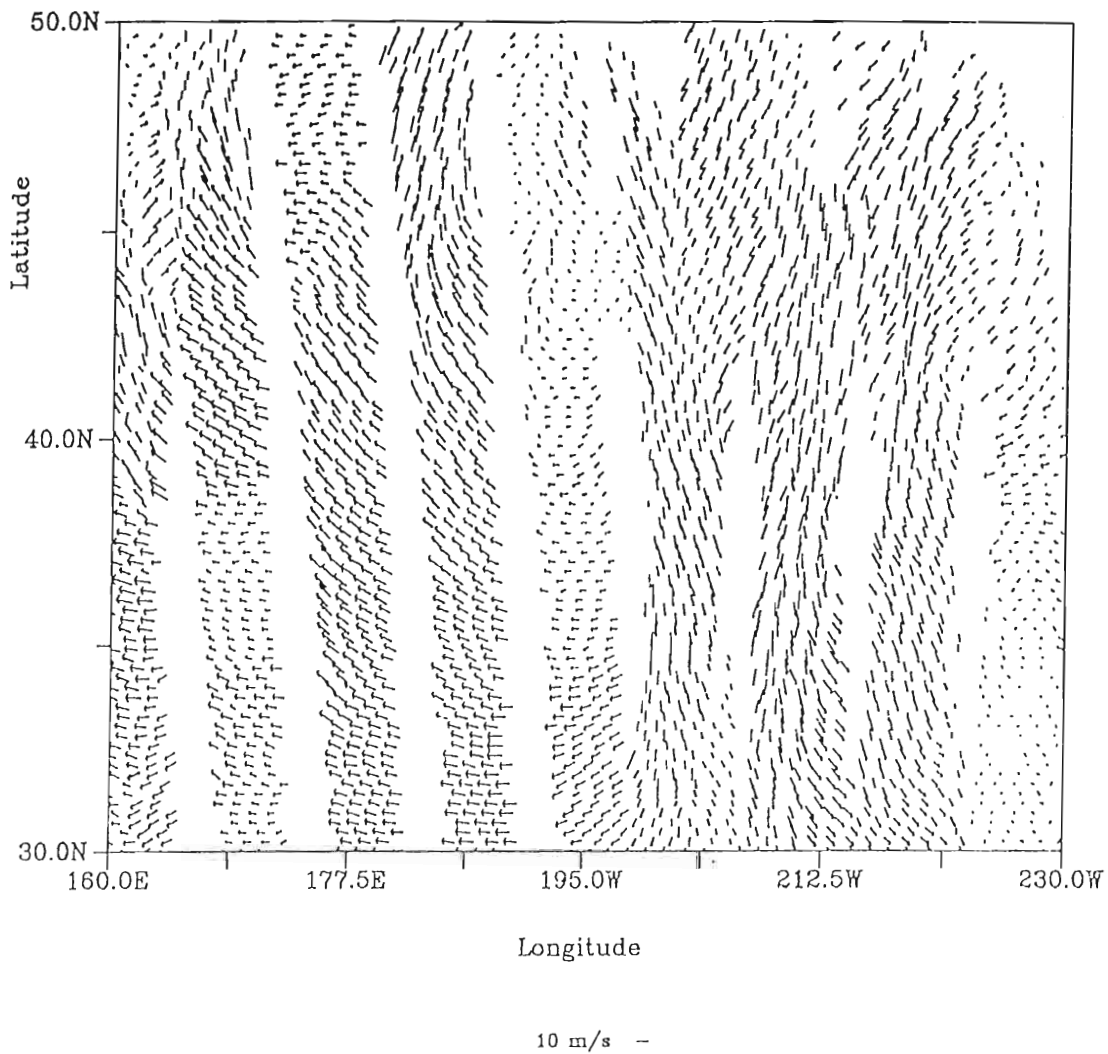
Fig. 5-22: Vector average of reconstructed scatterometer wind field using the first 8 ascending and descending EOFs for the period of 9-11 February 1992. Every 5th vector plotted.

latitude) would be void of observations. The combined three day field provides a exceptionally dense observation network, Table 5-4.

TABLE 5-4: The scatterometer wind field coverage under optimum conditions.

Data Field	Percent Coverage
Ascending	70
Descending	70
Synthesized	95

Current data assimilation techniques have demonstrated distinct improvements in AGCM forecasts when scatterometer winds have been incorporated; *e.g.*, Anderson *et al.* (1986) and Atlas (1994). The work of Barnier *et al.* (1993) evaluated the impact of the band-like sampling of satellite scatterometers on the ability of the scatterometer winds to force an ocean model. His results noted a strong similarity between the seasonal ocean circulations forced with scatterometer measurements (based on rapid repeat cycles) and reference winds (ECMWF model analysis of the 10m winds) with the perturbations from the band-like sampling and the persistence assimilation demonstrating similarity to the impact of adding small uncorrelated noise to the reference winds. The reconstructed wind fields from the present study (employing only the significant EOFs) provide a dense network of observations. These three day fields still retain the satellite sampling characteristics evident in the individual ascending and descending data sets but contain additional information, a measure of the steadiness evident in the flow.

evident in the flow.

6. Conclusion

In summary, the ERS-1 satellite provides the first spaceborne scatterometer measurements since SEASAT. The ERS-1 instrumentation clearly employs the lessons of SEASAT featuring an improved antennae and frequency design. The three antennae layout allows for an exact solution to the ambiguity selection problem in the absence of measurement and model error (Schultz, 1990). Further, the 5.3 GHz frequency implantation demonstrates only limited σ° degradation in the presence of precipitation (Quilfen *et al.*, 1993).

This study examines the information content of the three day repeat orbit scatterometer winds and utilizes the wind vector ambiguity determined by the CMODFD / NSCAT MLE algorithm. The study methodology employs a separate comparative and EOF analysis on the ascending and descending orbit wind data. Comparative fields are primarily the ECMWF/TOGA model analysis.

The scatterometer wind retrieval algorithm (CMODFD / NSCAT MLE) performed reasonably well throughout the study period but does demonstrate some problems. This assessment is based on subjective analysis, interswath comparisons, and correlations with the ECMWF model analysis. The results indicate the difficulties in the ambiguity selection are more pronounced in the descending orbits. Most of the difficulties cited in both data sets (ascending an descending) appear to be related to the ambiguity selection are more pronounced in the descending orbits. Most of the difficulties cited in both data sets (ascending an descending) appear to be related to upwind-downwind symmetry problems. In general, erroneous ambiguity selections are

61

readily identifiable by inspection.

As expected, the scatterometer derived winds provide detail to the existing wind structures for scales smaller than 2° latitude and/or longitude. The comparative results depict generally good agreement between the ERS-1 and ECMWF wind fields but distinct, non-isolated differences are noted. These difficulties include the center positioning (characteristic of the ascending data), generally stronger wind speeds and more well-defined curvature in scatterometer cyclonic and coll regions, and contrasts in the overall scale of various atmospheric wind patterns. The differences in center positioning depict the ECMWF-located cyclonic center north of the scatterometer center position and is found in approximately 90% of the patterns reviewed. Placement varies between cyclonic patterns and ranges from 1-3° latitude. The differences demonstrated in the speed structure and curvature coupled with the smaller scale features are likely to be reflected in the vorticity fields computed from the ECMWF and ERS-1 velocity fields. The limited study results support this conjecture depicting small regions of the scatterometer derived vorticity fields with vorticity magnitudes 25-50% greater than presented in the ECMWF derived vorticity fields.

The qualitative results from comparisons of ECMWF monthly and three month means to the corresponding scatterometer means demonstrate poor agreement between the data sets for the month of January with the magnitudes of the scatterometer winds generally stronger and directional correspondence providing only vague agreement. The two data sets demonstrate a greater correspondence during the months of February and March, improving over the period. This improvement reflects the increased

62

scatterometer observations and possibly the effects of improved calibration and/or less monthly variability as compared to the month of January; hence making it easier to correlate the two wind fields. The three month mean demonstrates good agreement with the ECMWF mean and climatology. The rms differences between the ECMWF and ERS-1 three month mean wind field computed in the study were 1.28ms^{-1} / 16.7° and 0.96ms^{-1} / 22.44° for the ascending-ECMWF and descending-ECMWF comparisons, respectively. These results compare favorably with those presented by Halpern *et al.* (1992).

The EOF results partition the sampled variance in the ascending and descending wind data and suggest the more significant spatial/temporal EOFs depict definable frequency divisions. The study results suggest periods of 18-21 days, 8-10 days, and 6-8 days. These reflect the time scales associated with the planetary wave cycle, large scale general circulation systems, and smaller scale storm structures, respectively, in the mid-latitudes (Barry *et al.*, 1987 and Carlson, 1991). The first four EOFs, those for which the results suggest physically motivated phenomena, account for 50-60% of the total variance sampled in the data. Employing this partitioning of the variance as a filtering mechanism demonstrates only limited capability in removing erroneous wind vectors and is generally inadequate in eliminating upwind-downwind symmetry errors.

The combined three day wind fields provide dense spatial coverage over the study region (~90%). These fields still retain the much of the sampling characteristics found in the individual ascending and descending data sets (irregularly sample in time study region (~90%). These fields still retain the much of the sampling characteristics found in the individual ascending and descending data sets (irregularly sample in time

across satellite swaths) but contain additional information (at the coincident ascending / descending grid points) on the measure of the steadiness exhibited in the winds. Further, using the EOF analysis technique to partition the variance, two wind vectors, one from the ascending and descending orbits, reconstructed from a limited number of EOFs can be combined without seriously degrading the three day variability sampled in the individual data sets.

Current data assimilation techniques have resulted in distinct improvements of AGCM forecasts when scatterometer winds have been incorporated; *e.g.*, Anderson *et al.* (1986) and Atlas (Personal communications, 1994). For ocean processes, the work of Barnier *et al.* (1993) notes a strong similarity between the ocean circulations driven by simulated scatterometer winds and ECMWF analysis winds, used as reference winds. Additionally, he notes the "band-like" sampling of the scatterometer produces perturbations are similar to the impact of adding small uncorrelated noise to reference winds. The reconstructed three day wind fields from the present study may help, particularly in regions where the persistence of the winds are greater than three days (exceeding the satellite ground track repeatability). These combined three day wind fields employ only the significant EOFs and provide a dense observational network over the three repeat cycle. These wind fields retain the longer time scale variability. In effect, retention of only the significant EOFs appears to remove the variability contributed by the shorter time scales, *i.e.*, variability (atmospheric phenomena) sampled in only one or two satellite swaths (1-3 days).

The work and results of this study highlight several areas deserving of

64

continued research. The research opportunities associated with ambiguity selection provide promising prospects as does continued work into the development of three day wind fields for possible oceanographic applications. Ongoing research into the impact of assimilated ERS-1 scatterometer winds on AGCM forecasts, *e.g.* Atlas (Personal communications, 1994), clearly illustrate a positive impact in the southern hemisphere but only of limited influence in the northern hemisphere. Much of the new information scatterometer winds provide exists at scales beyond the resolvability of many AGCMs (*i.e.*, smaller than the 2 delta x limitations dictated in the Sampling Theorem, limitations driven by computational stability, and/or limitations in the assimilation methodology). This "lost" information provides a cornucopia of related research topics and interests for future work, *e.g.* frontal location and dynamics, small scale atmospheric and oceanographic dynamics, *etc.*

In conclusion, the ERS-1 three day repeat orbit winds provide useful information on atmospheric time scales from 7-21 days and length scales from 700 - 5000 km. These measurements are a rich source of data capable of resolving atmospheric wind structures smaller than 100 km and providing valuable information in otherwise data sparse regions. The greater spatial resolution, enhanced small scale structure, and observed reliability illustrate the ERS-1 scatterometer wind fields represent a significant data source for operational and research use. Coupled with the continuing improvements in wind retrieval algorithms and ambiguity selection schemes, the ERS-1 scatterometer data will only serve to strengthen the utility and continuing improvements in wind retrieval algorithms

schemes, the ERS-1 scatterometer data will only serve to strengthen the utility and functionality of remote sensing.

References

Amans, V. and B. Marcorelles, *AMI unavailability periods since launch*, DEX/EM/92-10-002, European Space Agency, 1993.

Anderson, D., A. Hollingsworth, S. Uppala, and P. Woiceshyn, A study of the feasibility of using sea and wind information from the ERS-1 satellite, 1, Wind scatterometer data, ESRIN contract 6297/86/HGE-I(SC), 121 pp., Eur. Cent. for Medium-Range Forecasts, Berkshire, England, 1987.

Barnier, B., J. Capella, and J. J. O'Brien, The use of satellite scatterometer winds to drive a primitive-equation model of the Indian ocean: the impact of the band-like sampling,to appear *J. Geophys. Res.*, 1994.

Barry, R. G. and R. J. Chorley, *Atmosphere, weather, & climate*, 5th Ed., 460 pp., 141-195, 1987.

Boer, G. J. and T. G. Shephard, Large-scale two-dimensional turbulence in the atmosphere, *J. Atmos. Sci.*, 40, 164-184, 1983.

Brown, R. A., On a satellite scatterometer as an anemometer, *J. Geophys. Res.*, 88(C3), 1663-1673, 1983.

Carlson, T. N., *Mid-latitude weather systems*, 507pp, 1991.

Estoque, M. A., and J. Feranadez-Partagas, *Subsynoptic variations in seasat wind, Scientific Report*, UM RSMAS No. 83016, Sept 1983.

Freilich, M. H., and R. S. Dunbar, A C-band scatterometer model function from ERS-1 and global surface analysis data: 1992 ADEOS/NSCAT science team meeting, Hakone, Japan, 689pp, 1992.

Freilich, M. H., and D. B. Chelton, Wavenumber spectra of Pacific winds measured by the Seasat scatterometer, *J. Phys. Oceanogr.*,16, 741-757, 1986.

the Seasat scatterometer, *J. Phys. Oceanogr.*,16, 741-757, 1986.

Halpern, D., W. Knauss, O. Brown, and F. Wentz, *An Atlas of monthly mean distributions of SSMI surface wind speed, ARGOS buoy drift, AVHRR/2 sea surface temperature, and ECMWF surface wind components during 1991*, JPL Publication 93-10, Jet Propulsion Laboratory, Pasadena, 111 pp. 1993a.

Halpern, D., M. H. Frielich, and R. S. Dunbar, Evaluation of two January - June 1992 ERS-1 AMI wind vector data sets, Proceedings first ERS-1 symposium, *Space at the service of our environment*, ESA SP 359, March 1993b.

Hellerman, S. and M. Rosenstein, Normal monthly wind stress over the world ocean with error estimates, *J. Phys. Oceanogr.*, 13, 1093-1105, 1983.

Hoffman, R. N., *A preliminary study of the impact of C-band scatterometer wind data on global scale numerical weather prediction*, Tech Report 69, European Center for Medium-Range Weather Forecasts, Nov 1992.

Janssen, P., Lionello, P., Reistad, M., and A. Hollingsworth, *A study of the feasibility of using sea and wind information from the ERS-1 satellite, 2, Use of scatterometer and altimeter data in wave modelling and assimilation*, ESRIN contract 6297/86/HGE-I(SC), 108 pp., European Center for Medium-Range Forecasts, Berkshire, England, 1987.

Jones, C. S., D. M. Legler, and J. J. O'Brien, Variability of surface fluxes over the Indian Ocean; 1960-1989, to appear *Atmos. Ocean Sys.*, 1994.

Katsaros, K. B., and R. A. Brown, Legacy of the SEASAT mission for studies of the atmosphere and air-sea-ice interactions, *Bull. Am. Meteorol. Soc.*, 72(7), 967-979, 1991.

Legler, D. M. and J. J. O'Brien, Objectively analyzed air-sea flux fields using a combination of in-situ and remotely sensed data, to appear *J. Geophys. Res. - Oceans*, 1994

Legler, D. M. and J. J. O'Brien, Development and testing of a simple assimilation technique to derive average wind fields from simulated scatterometer data, *Mon. Wea. Rev.*, 113, 1791-1800, 1985.

Legler, D. M., Empirical orthogonal function analysis of wind vectors over the tropical Pacific region. *Bull. Amer. Meteor. Soc.*, 64, 234-241, 1983.

Liou, K. N., *An introduction to atmospheric radiation*, University of Utah, Salt Lake City, Utah, 392 pp., 1980

Liou, K. N., *An introduction to atmospheric radiation*, University of Utah, Salt Lake City, Utah, 392 pp., 1980

Miles, K. F., D. M. Legler, and J. J. O'Brien, Variability of five day wind fields over the Indian Ocean using ship and SASS data, to appear *Atmos. Ocean Sys.*, 1994.

O'Brien, J. J. (Chairman), *Scientific opportunities using satellite wind stress measurements over the ocean: Report of the satellite surface stress working group*, NAS5-26714, 153 pp., 1982.

Oberhuber, J. M., *An atlas based on the COADS data set: The budgets of heat, buoyancy and turbulent kinetic energy at the surface of the global ocean*, Max-Plank-Institut für Meteorologie, Hamburg, Germany, 100pp, 1988.

Preisendorfer, R. W., *Developments in atmospheric science 17: Principal component analysis in meteorology and oceanography*, 425 pp., 1988.

Press, W. H., S. A. Teukolsky, W. T. Vetterling, and B. P. Flannery, *Numerical recipes in FORTRAN: The art of scientic computing*, 963 pp., 1992.

Quilfen, Y., K. B. Katsaros, and B. Chapron, Surface wind and precipitation patterns in tropical cyclones observed with the ERS-1 scatterometer and with the special sensor mircowave/imager: Proceedings second ERS-1 symposium, *Space at the service of our environment*, ESA SP 361, 2, 1993.

Schultz, H., A circular median filter approach for resolving directional ambiguities in wind fields retrieved from spaceborne scatterometer data, *J. Geophys. Res.*, 95(C4), 5291-5303, 1990.

Slutz, R. J., S. J. Lubker, J. D. Hiscox, S. D. Woodruff, R. L. Jenne, D. H. Joseph, P. M. Steurer, and J. D. Elms, *COADS Comprehensive Ocean-Atmosphere Data Set Release 1*, CIRES University of Colorado. 300 pp., 1985.

Stoffelen, A. and D. L. T. Anderson, ERS-1 scatterometer calibration and validation activities at ECMWF: A. The quality and characteristics of the radar backscatter measurements. In: *Proceedings of the ERS-1 Geophyiscal Validation Campaign RENE 1991, Penhors, 27 - 30 April 1992*, European Space Agency, Paris, 83-88, 1992

Stricherz, J. N., D. M. Legler, and J. J. O'Brien, *Atlas of Florida State University Indian Ocean winds for TOGA 1970-1985*, Florida State University, Tallahassee, FL, 216 pp., 1993.

Trenberth, K. E., W. G. Large and J. G. Olson, The mean annual cycle in global ocean Tallahassee, FL,'zro pp.;"1993. 20 1742 1760 1990

Trenberth, K. E., W. G. Large and J. G. Olson, The mean annual cycle in global ocean wind stress, *J. Phys. Oceanogr.*, 20, 1742-1760, 1990.

Wright, P. B., *An atlas based on the COADS data set: Fields of mean winds, cloudiness and humidity at the surface of the global ocean*, Max-Plank-Institut für Meteorologie, Hamburg, Germany, 50pp, 1988.

Biographical Sketch

Paul Beaudoin was born in Pensacola, Fl. on January 11, 1964. The first of three children born to Paul and Mary Beaudoin. He graduated from New Castle High School in June 1982 and graduated from the School of Engineering at the University of Virginia in May 1986 thereby accepting a commission in the United States Air Force. He completed the USAF Basic Meteorology Program at Florida State University in May 1988. While studying at FSU, he met and latter married a charming young lady, Helen E. Middleton. Paul completed two tours with the USAF, the first at Seymour Johnson AFB, North Carolina, and the second in Stuttgart, Germany, providing environmental support to the Deputy Commander of the United States Forces in Europe. While in Germany, Mary C. Beaudoin was born to Paul and Helen. In December 1992, Paul returned to civilian life and to Florida State University where he completed his Master of Science in meteorology in August of 1994. Upon completion of the M.S., Paul and his family will move to Maryland where Paul will begin work at NASA Goddard.